J|A|C|S
ARTICLES
Published on Web 01/17/2007

Aryl-Fluoride Reductive Elimination from Pd(II): Feasibility Assessment from Theory and Experiment

Dmitry V. Yandulov* and Ngon T. Tran

Contribution from the Department of Chemistry, Stanford University, Stanford, California 94305-5080

Received September 30, 2006; E-mail: yandulov@stanford.edu

Abstract: DFT methods were used to elucidate features of coordination environment of Pd(II) that could enable Ar−F reductive elimination as an elementary C−F bond-forming reaction potentially amenable to integration into catalytic cycles for synthesis of organofluorine compounds with benign stoichiometric sources of F^-. Three-coordinate T-shaped geometry of $Pd^{II}Ar(F)L$ (L = NHC, PR_3) was shown to offer kinetics and thermodynamics of Ar−F elimination largely compatible with synthetic applications, whereas coordination of strong fourth ligands to Pd or association of hydrogen bond donors with F each caused pronounced stabilization of Pd(II) reactant and increased activation barrier beyond the practical range. Decreasing donor ability of L promotes elimination kinetics via increasing driving force and *para*-substituents on Ar exert a sizable S_NAr-type TS effect. Synthesis and characterization of the novel $[Pd(C_6H_4\text{-}4\text{-}NO_2)ArL(\mu\text{-}F)]_2$ (L = P(*o*-Tolyl)$_3$, **17**; P(*t*-Bu)$_3$, **18**) revealed stability of the fluoride-bridged dimer forms of the requisite $Pd^{II}Ar(F)L$ as the key remaining obstacle to Ar−F reductive elimination in practice. Interligand steric repulsion with P(*t*-Bu)$_3$ served to destabilize dimer **18** by 20 kcal/mol, estimated with DFT relative to PMe_3 analog, yet was insufficient to enable formation of greater than trace quantities of Ar−F; C−H activation of P(*t*-Bu)$_3$ followed by isobutylene elimination was the major degradation pathway of **18** while Ar/F^- scrambling and Ar−Ar reductive elimination dominated thermal decomposition of **17**. However, use of Buchwald's L = $P(C_6H_4\text{-}2\text{-}Trip)(t\text{-}Bu)_2$ provided the additional steric pressure on the $[PdArL(\mu\text{-}F)]_2$ core needed to enable formation of aryl-fluoride net reductive elimination product in quantifiable yields (10%) in reactions with both **17** and **18** at 60° over 22 h.

Introduction

Fundamental advances in understanding and controlling reactivity of organometallic complexes have paved the way for the emergence of versatile cross-coupling synthetic methods, a plethora of which currently enable efficient synthesis of carbon−carbon and carbon−heteroatom (X═B, Si, P, N, S, O) bonds by means of late transition metal catalysis.[1] Fluorine stands out as an attractive target for the development of analogous catalytic C−F bond-forming protocols, whereas traditional−stoichiometric−organofluorine chemistry continues to challenge synthetic chemists and demand specialized expertise.[2,3,4] The prospects of developing catalytic methods of C−F bond synthesis, specifically those that rely on the more benign of the fluorine sources such as alkali metal fluorides with phase-transfer catalysis (PTC), yet accomplish synthetic tasks ordinarily associated with hazards and expenses of anhydrous HF (AHF) and/or electrophilic fluorinating reagents, are underscored by the ever-expanding utilization of fluorine functionality in biologically active compounds[5,2] and materials.[3] Key to realization of such catalytic fluorination approaches is the development of elementary transition metal-mediated C−F bond forming reactivity, specifically that compatible with alkali MF/PTC as the in situ source of stoichiometric F^-. Combination of such reactivity with the various mechanisms of activation and transformation of organic substrates established broadly across transition metal series in the context of numerous catalytic cycles[1] potentially could reduce experimental hazards involved in syntheses of many organofluorine compounds to a routine level and improve their accessibility.

(1) (a) *Transition Metals for Organic Synthesis: Building Blocks and Fine Chemicals*; Beller, M., Bolm, C., Eds.; Wiley-VCH: Weinheim, 2004. (b) *Applied Homogeneous Catalysis with Organometallic Compounds : A Comprehensive Handbook in Three Volumes*; Cornils, B., Herrmann, W. A., Eds.; Wiley-VCH: Weinheim, 2002. (c) *Handbook of Organopalladium Chemistry for Organic Synthesis*; Negishi, E. I., Ed.; Wiley-Interscience: New York, 2002. (d) *Compounds with Transition Metal−Carbon p-Bonds and Compounds of Groups 10−8 (Ni, Pd, Pt, Co, Rh, Ir, Fe, Ru, Os)*; Lautens, M., Ed.; Science of Synthesis: Houben Weyl Methods of Molecular Transformations, Vol. 1; Thieme: New York, 2000. (e) *Top. Organomet. Chem.* **2005**, *14*.

(2) *Organo-Fluorine Compounds*; Baasner, B., Hagemann, H., Tatlow, J. C., Eds.; Methods of Organic Chemistry (Houben-Weyl), Vol. E10; Thieme Verlag: Stuttgart, 1999.

(3) *Organofluorine Chemistry: Principles and Commercial Applications*; Banks, R. E., Smart. B. E., Tatlow, J. C., Eds.; Plenum Press: New York, 1994.

(4) (a) Hiyama, T. *Organofluorine Compounds: Chemistry and Applications*; Springer: New York, 2000. (b) Hiyama, T.; Shimizu, M. *Angew. Chem., Int. Ed.* **2005**, *44*, 214−231. (c) Ma, J.-A.; Cahard, D. *Chem. Rev.* **2004**, *104*, 6119−6146. (d) *Top. Curr. Chem.* **1997**, *193*. (e) Wilkinson, J. A. *Chem. Rev.* **1992**, *92*, 505−519.

(5) (a) Jeschke, P. *ChemBioChem* **2004**, *5*, 570−589. (b) Pesenti, C.; Fiorenza Viani, F. *ChemBioChem* **2004**, *5*, 590−613. (c) Ojima, I. *ChemBioChem* **2004**, *5*, 628−635. (d) Böhm, H.-J.; Banner, D.; Bendels, S.; Kansy, M.; Kuhn, B.; Müller, K.; Obst-Sander, U.; Stahl, M. *ChemBioChem* **2004**, *5*, 637−643. (e) *Biomedical Frontiers of Fluorine Chemistry*; Ojima, I., McCarth, J. R., Welch, J. T., Eds.; ACS Symposium Series 639; American Chemical Society: Washington, DC, 1996.

10.1021/ja066930l CCC: $37.00

Several distinct mechanistic scenarios in which a metal mediates the formation of a carbon−fluorine bond have been categorized,[3] although definitive mechanistic studies are few.[6] By far the most common elementary pathway is nucleophilic substitution at carbon by F^- accompanied to a varying degree by electrophilic assistance from the metal in abstracting the nucleofuge. This category spans the full range of mechanisms from limiting $A_N + D_N$,[7] through A_ND_N (S_N2) to limiting $D_N + A_N$ (S_N1) that broadly characterize halide exchange fluorination reactivity of binary metal fluorides with aliphatic, vinylic, aromatic, and carbonyl substrates.[2] Performing best in such reactions under strongly acidic conditions,[8] most commonly used fluorides[2] of V^V, $Cu^{II,II/0}$, Ag^I, Zn^{II}, $Hg^{I,II}$, Tl^I, Pb^{II}, As^{III}, $Sb^{III,V}$ are suited ideally for catalysis of halide exchange fluorinations with AHF medium,[2] rather than with alkali MF/PTC, which has been claimed.[9] Although lattice energies[10] suggest that some of the above binary fluorides can be formed by halide exchange of heavier halide salts with alkali MF, treatment of corresponding oxides/hydroxides with HF remains the most practical preparative route to these historically stoichiometric fluorinating agents that is also used to prepare alkali MF.[2] Well-defined η^1-I iodoalkane organometallic complexes of Re^I and Ru^{II} display mechanistically related reactivity in yielding corresponding fluoroalkanes with alkali MF/PTC among other F^- sources.[11] Although competing displacement of intact RI with F^- underlines the general challenge of maintaining a substrate between a strong Lewis acid and a nucleophilic F^-, successful development of halide exchange fluorination of aliphatic halides with TlF *catalytic* in $[Ru^{II}ClP_2L_2]^+$ (L = P or N donor) complexes of Togni et al.[12] stresses the existence of a useful range of compatible catalyst Lewis acidity and F^- nucleophilicity.

Oxidative formation of C−F bonds comprises the other major metal-mediated mechanistic category. A number of high(est) oxidation state binary metal fluorides,[2,13] including heterogeneous NiF_x anode phases featured in electrochemical fluorination,[2,3] effect oxidative fluorinations of a wide range of hydrocarbons and other substrates, in which MF_n reagent is commonly accepted to[6c,3] effect single electron-transfer oxidation(s), subsequently providing, together with AHF medium where applicable, F^- to the resulting cationic intermediates. Following the pioneering work of Togni et al. on asymmetric fluorination of β-keto esters[14] with chiral Ti^{IV}(TADDOLate)-X_2 catalysts,[15a,b] Sodeoka[15c,d] and Cahard[15e,f] developed well-defined Pd^{II}, Cu^{II}, and other metal-based catalytic systems, in all of which C−F bond formation is believed to result from direct electrophilic attack at chiral metal-bound enolate intermediates by stoichiometric $[N-F]^+$ electrophilic fluorinating reagents. Most recently, Sanford et al. reported on directed oxidative fluorination of unactivated aromatic and aliphatic C−H bonds with electrophilic $[N-F]^+$ reagents catalyzed by $Pd(OAc)_2$,[16a] expanding on the extensive range of well-defined C−O bond-forming oxidative transformations developed with the same system.[16b−e] Ultimately reliant on stoichiometric F_2 and/or AHF, none of the above oxidative C−F bond forming processes are readily amenable to integration into alkali MF-based catalytic fluorination cycles. However, combination of a F^- source with chemical,[17,4,a,b,2] electrochemical,[2,3] or photochemical[18] oxidation continues to offer promising opportunities for the development of less hazardous alternatives to the use of elemental F_2.

The only known catalytic fluorination process that converts alkali MF into "advanced" organofluorine compounds, not accessible from alkali MF directly, is the carbonylative halide exchange fluorination of aryl halides (fluorocarbonylation, eq 1),[19] performed first under relatively mild conditions by Tanaka et al.[20]

$$\underset{X\neq F;\ M=\text{alkali}}{Ar-X + CO + MF/PTC} \xrightarrow[PR_3,\ \Delta]{\text{cat. } Pd^{II}} ArC(O)F + MX \quad (1)$$

Subsequent reactivity studies by Grushin[21] suggested reductive elimination of ArC(O)−F from Pd^{II} as the mechanism of C−F bond formation in this system, by analogy to the reductive elimination of other carboxylic acids derivatives mediating Pd^{II} catalysis of the many related carbonylative transformations of aryl halides.[22]

The unique catalytic fluorination system in eq 1 demonstrates viability of alkali MF as the in situ source of F^- in a Pd^{II}-mediated C−F bond-forming process potentially involving distinct Pd−F intermediates. Additional elementary C−F bond

(6) (a) San Filippo, J., Jr.; Romano, L. J. *J. Org. Chem.* **1975**, *40*, 782−787. (b) Bloodworth, A. J.; Bowyer, K. J. *Tetrahedron Lett.* **1987**, *28*, 5347−5350. (c) Burdon, J.; Parsons, I. W. *Tetrahedron* **1980**, *36*, 1423−1433.
(7) Smith, M. B.; March. J. *March's Advanced Organic Chemistry: Reactions, Mechanisms and Structure*; Wiley-Interscience: New York, 2001.
(8) For a notable exception, see: Pogány, S. A.; Zentner, C. M.; Ringeisen, C. D. *Synthesis* **1987**, 718−719.
(9) Grushin, V. V. U.S. Patent Application 111244,980, Oct. 5, 2005.
(10) *CRC Handbook of Chemistry and Physics, Internet Version 2007 (87th Edition)*; Lide, D. R., Ed.; Taylor and Francis: Boca Raton, FL, 2007.
(11) (a) Powell, J.; Horvath, M. J. *Organometallics* **1993**, *12*, 4067−4072. (b) Kulawiec, R. J.; Faller, J. W.; Crabtree, R. H. *Organometallics* **1990**, *9*, 745−755.
(12) (a) Barthazy, P.; Togni, A.; Mezzetti, A. *Organometallics* **2001**, *20*, 3472−3477. (b) Barthazy, P.; Stoop, R. M.; Wörle, M.; Togni, A.; Mezzetti, A. *Organometallics* **2000**, *19*, 2844−2852. (c) Barthazy, P.; Hintermann, L.; Stoop, R. M.; Wörle, M.; Mezzetti, A.; Togni, A. *Helv. Chim. Acta* **1999**, *82*, 2448−2453. (d) Becker, C.; Kieltsch, I.; Broggini, D.; Mezzetti, A. *Inorg. Chem.* **2003**, *42*, 8417−8429.
(13) Dukat, W. W.; Holloway, J. H.; Hope, E. G.; Rieland, M. R.; Townson P. J.; Powell, R. L. *J. Chem. Soc., Chem. Commun.* **1993**, 1429−1430.
(14) (a) Ma, J.-A.; Cahard, D. *Chem. Rev.* **2004**, *104*, 6119−6146. (b) Oestreich, M. *Angew. Chem., Int. Ed.* **2005**, *44*, 2324−2327. (c) Muñiz, K. *Angew. Chem., Int. Ed.* **2001**, *40*, 1653−1656.
(15) (a) Hintermann, L.; Togni, A. *Angew. Chem., Int. Ed.* **2000**, *39*, 4359−4362. (b) Piana, S.; Devillers, I.; Togni, A.; Rothlisberger, U. *Angew. Chem., Int. Ed.* **2002**, *41*, 979−982. (c) Hamashima, Y.; Yagi, K.; Takano, H.; Tamas, L.; Sodeoka, M. *J. Am. Chem. Soc.* **2002**, *124*, 14530−14531. (d) Hamashima, Y.; Takano, H.; Hotta, D.; Sodeoka, M. *Org. Lett.* **2003**, *5*, 3225−3228. (e) Ma, J.-A.; Cahard, D. *Tetrahedron: Asymmetry* **2004**, *15*, 1007−1011. (f) Ma, J.-A.; Cahard, D. *J. Fluorine Chem.* **2004**, *125*, 1357−1361.
(16) (a) Hull, K. L.; Anani, W. Q.; Sanford, M. S. *J. Am. Chem. Soc.* **2006**, *128*, 7134−7135. (b) Dick, A. R.; Sanford, M. S. *Tetrahedron*, **2006**, *62*, 2439−2463. (c) Deprez, N. R.; Kalyani, D.; Krause, A.; Sanford, M. S. *J. Am. Chem. Soc.* **2006**, *128*, 4972−4973. (d) Desai, L. V.; Malik, H. A.; Sanford, M. S. *Org. Lett.* **2006**, *8*, 1141−1144. (e) Dick, A. R.; Kampf, J. W.; Sanford, M. S. *J. Am. Chem. Soc.* **2005**, *127*, 12790−12791.
(17) Subramanian, M. A.; Manzer, L. E. *Science* **2002**, *297*, 1665.
(18) (a) Lai, C.; Kim, Y. I.; Wang, C. M.; Mallouk, T. E. *J. Org. Chem.* **1993**, *58*, 1393−1399. (b) Habibi, M. H.; Mallouk, T. E. *J. Fluorine Chem.* **1991**, *51*, 291−294. (c) Wang, C. M.; Mallouk, T. E. *J. Am. Chem. Soc.* **1990**, *112*, 2016−2018.
(19) (a) Prichard, W. W. U.S. Patent 2696503, 1954. (b) Mador, I. L.; Scheben, J. A. U.S. Patent 3452090, 1969. (c) Prichard, W. W. U.S. Patent 3632643, 1972.
(20) (a) Sakakura, T.; Chaisupakitsin, M.; Hayashi, T.; Tanaka, M. *J. Organomet. Chem.* **1987**, *334*, 205−211. (b) Okano, T.; Harada, N.; Kiji, J. *Bull. Chem. Soc. Jpn.* **1992**, *65*, 1741−1743. (c) Hatanaka, Y.; Fukushima, S.; Hiyama, T. *Tetrahedron* **1992**, *48*, 2113−2126.
(21) (a) Fraser, S. L.; Antipin, M. Yu.; Khroustalyov, V. N.; Grushin, V. V. *J. Am. Chem. Soc.* **1997**, *119*, 4769−4770. (b) Grushin, V. V. *Chem.−Eur. J.* **2002**, *8*, 1007−1014.
(22) (a) Komiya, S.; Akai, Y.; Tanaka, K.; Yamamoto, T.; Yamamoto, A. *Organometallics* **1985**, *4*, 1130−1136. (b) Grushin, V. V.; Alper, H. *J. Am. Chem. Soc.* **1995**, *117*, 4305−4315. (c) Grushin, V. V.; Alper, H. *Chem. Rev.* **1994**, *94*, 1047−1062. (d) Grushin, V. V.; Alper, H. *Top. Organomet. Chem.* **1999**, *3*, 193−226.

forming reactions mediated by transition metals may thus be envisioned that, taking advantage of the existing mechanisms by which various organic substrates can be transformed in a catalytic cycle,[1] could ultimately enable their functionalization into diverse organofluorine products in an expedient and versatile manner that poses few of the traditional hazards of organofluorine chemistry. As formulated earlier by Grushin,[21b] reductive elimination of alkyl- and aryl-fluorides is one such elementary reaction that appears especially promising as a nearly "drop-in" substitute for the product-forming step in the existing and widely utilized carbon−heteroatom (X = N, O, S, P) cross-coupling protocols.[1] As of yet, no examples of such elementary processes have been described in the literature,[23] with the most recent report by Sanford et al.,[16a] possibly signifying its operation from a Pd(IV) state.

Extensive precedent of closely related R−X reductive elimination reactivity − in particular with X = OR,[24] including most recently X = OH,[24h] as well as with X = Cl, Br and I,[25] and possibly X = F in the catalytic system of eq 1[19,20,21]—together with vast existing array of substrate activation and modification options available for both Pd(0) and Pd(II) states[1] makes palladium(II) coordination environment arguably the most promising platform on which to develop R−F reductive elimination reactivity. Pursuing such goals in the context of a novel catalytic approach to fluoroaromatics, Grushin's systematic studies of organometallic fluorides of Pd(II) produced the first examples of the surprisingly covalent and stable bonding between the soft Pd(II) center and the hardest base, F^-, in a series of isolated and fully characterized molecular complexes.[21,26] Remarkably, though exhibiting several unique reactivity modes,[21a,26a−d,f] the novel Pd(II) fluorides of varied structure and composition were found invariably stable to reductive elimination of aryl fluorides, evolving instead under forcing conditions via P−F and P−C reductive elimination.[21b,26e,g,h]

Given the difficulty of direct experimental approaches to produce the desired R−F reductive elimination reactivity with Pd(II), in the present study we undertook a computational (DFT) assessment of thermodynamic and kinetic feasibility of this process taking place from Pd(II) coordination environments featured in related catalytic transformations. Predicted absolute activation and equilibrium thermochemistry suggests that prospects of aromatic C−F reductive elimination from Pd(II) are far from unreasonable when starting with a three-coordinate PdArF(L) geometry. Maintaining such unsaturated coordination environment in practice however, may be the key challenge to address experimentally: we find {Pd(C_6H_4-4-NO_2)F(P(*t*-Bu)$_3$)}, whose Br and I analogs exhibit unique three-coordinate geometries in solution and solid state,[25b,e] to exist as a fluoride-bridged dimer as does the novel [Pd(C_6H_4-4-NO_2)F(P(*o*-Tolyl)$_3$)]$_2$ at temperatures of up to 95 °C in solution. Stability of dimeric ground states even in these Pd(II) coordination environments of high degree of steric congestion ultimately limits the extent of Ar−F reductive elimination to trace levels, with overwhelming preference displayed for a plethora of conventional C−C, P−C, C−H, and P−F bond-forming/breaking decomposition pathways. Nevertheless, both isolated [Pd(C_6H_4-4-NO_2)L(μ-F)]$_2$ produce, in the presence of Buchwald's P(*t*-Bu)$_2$(C_6H_4-2-Trip), the sought F−C_6H_4-4-NO_2 in 10% yield over 22 h at 60 °C.

Results

A. Computational Studies. 1. Benchmark of the Computational Models. The computational models used in the studies of the as-yet unobserved processes of C−F reductive elimination from Pd(II) environments were tested on (*o*-Tolyl)-bromide reductive elimination equilibrium of Pd(*o*-Tolyl)Br(P(*t*-Bu)$_3$)/P(*t*-Bu)$_3$, thermodynamics and kinetics of which have been determined by Roy and Hartwig[25c,d] (Table 1).

Although most geometrical parameters are reproduced fairly well with both MO and ONIOM models (within 2.6% for overestimated Pd−P(*t*-Bu)$_3$ distances), the key difference from the experiment lies in the substantially longer single Pd···HC agostic bond featured in the optimized geometries. The inadequate description of the agostic interaction, which serves to stabilize Pd(II) state, may be the reason why equilibrium and activation free energies are underestimated by 0 (6) and 5 (6) kcal/mol with the best MO (ONIOM) models, which include solvation energies. It is notable that the Pd···HC distance is shorter in the ONIOM model, which describes the agostic interaction only approximately with electrostatic nonbonded term of the UFF energy of the real system, but represents adequately inter- and intraligand steric repulsion important in pushing the agostic C−H bond to Pd.[28] Within the limits of the above discrepancies, ONIOM performs adequately as compared to MO models, which reproduce experimental BDE's of Ph−F (125.6) and Ph−Cl (95.5)[10] as 123.4 and 93.3 kcal/mol, respectively (B3PW91/BS II //BS I). Being largely equivalent to the BS I energy/BS I geometry scheme otherwise, use of BS II single-point energies on BS I-optimized geometries reduced BSSE's in the energies of fluoride-bridged dimers to a negligible level and was therefore chosen as the standard approach. Computational data presented in the following can thus be considered accurate to within 5 kcal/mol relative to the experiment, with

(23) $ArTl^{III}F_2$ and $ArPb^{IV}(OAc)_3$ are known to yield corresponding ArF on treatment with BF_3, possibly in a manner of concerted reductive elimination from a high-valent organometallic fluoride intermediate; the incipient aryl cation character noted of the $ArTl^{III}F_2$ reactivity suggests fluoro-dediazoniation ($ArN_2^+ + F^- \rightarrow ArF$) as a closer mechanistic analogy for these reactions than a concerted Ar-F reductive elimination: (a) De Meio, G.; Morgan, J.; Pinhey, J. T. *Tetrahedron* **1993**, *49*, 8129−8138. (b) Taylor, E. C.; Bigham, E. C.; Johnson, D. K. *J. Org. Chem.* **1977**, *42*, 362−363.

(24) (a) Mann, G.; Hartwig, J. F. *J. Am. Chem. Soc.* **1996**, *118*, 13109−13110. (b) Widenhoefer, R. A.; Zhong, H. A.; Buchwald, S. L. *J. Am. Chem. Soc.* **1997**, *119*, 6787−6795. (c) Widenhoefer, R. A.; Buchwald, S. L. *J. Am. Chem. Soc.* **1998**, *120*, 6504−6511. (d) Mann, G.; Incarvito, C.; Rheingold, A. L.; Hartwig, J. F. *J. Am. Chem. Soc.* **1999**, *121*, 3224−3225. (e) Aranyos, A.; Old, D. W.; Kiyomori, A.; Wolfe, J. P.; Sadighi, J. P.; Buchwald, S. L. *J. Am. Chem. Soc.* **1999**, *121*, 4369−4378. (f) Mann, G.; Shelby, Q.; Roy, A. H.; Hartwig, J. F. *Organometallics* **2003**, *22*, 2775−2789. (g) Vorogushin, A. V.; Huang, X.; Buchwald, S. L. *J. Am. Chem. Soc.* **2005**, *127*, 8146−8149. (h) Anderson, K. W.; Ikawa, T.; Tundel, R. E.; Buchwald, S. L. *J. Am. Chem. Soc.* **2006**, *128*, 10694−10695.

(25) (a) Roy, A. H.; Hartwig, J. F. *J. Am. Chem. Soc.* **2001**, *123*, 1232−1233. (b) Stambuli, J. P.; Bühl, M.; Hartwig, J. F. *J. Am. Chem. Soc.* **2002**, *124*, 9346−9347. (c) Roy, A. H.; Hartwig, J. F. *J. Am. Chem. Soc.* **2003**, *125*, 13944−13945. (d) Roy, A. H.; Hartwig, J. F. *Organometallics* **2004**, *23*, 1533−1541. (e) Stambuli, J. P.; Incarvito, C. D.; Bühl, M.; Hartwig, J. F. *J. Am. Chem. Soc.* **2004**, *126*, 1184−1194.

(26) (a) Pilon, M. C.; Grushin, V. V. *Organometallics* **1998**, *17*, 1774−1781. (b) Grushin, V. V. *Angew. Chem., Int. Ed.* **1998**, *37*, 994−996. (c) Flemming, J. P.; Pilon, M. C.; Borbulevitch, O.; Ya Antipin M. Yu.; Grushin, V. V. *Inorg. Chim. Acta*, **1998**, *280*, 87−98. (d) Marshall, W. J.; Thorn, D. L.; Grushin, V. V. *Organometallics* **1998**, *17*, 5427−5430. (e) Grushin, V. V. *Organometallics* **2000**, *19*, 1888−1900. (f) Roe, D. C.; Marshall, W. J.; Davidson, F.; Soper, P. D.; Grushin, V. V. *Organometallics* **2000**, *19*, 4575−4582. (g) Grushin, V. V.; Marshall, W. J. *Angew. Chem., Int. Ed.* **2002**, *41*, 4476−4479. (h) Marshall, W. J.; Grushin, V. V. *Organometallics* **2003**, *22*, 555−562.

(27) Tanaka, M. *Acta Cryst.* **1992**, *C48*, 739−740.

(28) Ujaque, G.; Cooper, A. C.; Maseras, F.; Eisenstein, O.; Caulton, K. G. *J. Am. Chem. Soc.* **1998**, *120*, 361−365.

Table 1. Comparison of Various Computational Models in Describing Experimental Structures (Å, deg) and Energetics (kcal/mol) Pertaining to (*o*-Tolyl)-Br Reductive Elimination from Pd(*o*-Tolyl)Br(P(*t*-Bu)$_3$)

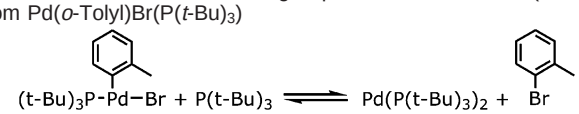

	Pd–P(*t*-Bu)$_3$	Pd–Ar	Pd–Br	CH···Pd[a]	P–Pd–Ar	Ar–Pd–X	$\Delta G^{\ddagger}_{+65\,°C}$	$\Delta G°_{+70°C}$
Pd(2,4-Xyl)I(P(*t*-Bu)$_3$)[b]	2.294(1)	1.982(4)		2.26	100.9(1)	94.0(1)		
PdPhBr(P(*t*-Bu)$_3$)[c]	2.2854(13)	1.977(5)	2.4537(8)	2.13	99.92(15)	93.14(5)		
Pd(P(*t*-Bu)$_3$)$_2$[d]	2.285(3)							
Pd(*o*-Tolyl)Br(P(*t*-Bu)$_3$)							24.1[e]	−0.8[f]
ONIOM[g]/BS I//BS I[h]	2.344/2.294[i]	1.968	2.410	2.41	103.1	96.0	15.8	−8.4
ONIOM/BS II//BS I[j]							15.7	−9.9
ONIOM/BS III//BS I[k]							15.7	−10.2
ONIOM/BS II//BS I + B3PW91/BS I/C_6H_6[l]							17.8	−7.0
B3PW91/BS I//BS I	2.349/2.332[i]	1.973	2.425	2.48	101.7	94.4	17.3	−2.4
B3PW91/BS II //BS I							17.0	−3.8
B3PW91/BS II //BS I + B3PW91/BS I/C_6H_6[l]							19.2	−1.0

[a] C−H bonds extended to 1.083 Å in X-ray structures. [b] CCDC structure code PABLOU, ref 25e. [c] CCDC structure code EROGUN, ref 25e. [d] CCDC structure code TARDUL, ref 27. [e] Computed from the value of 2.0×10^{-3} s^{-1} for rate constant k_1 of path **C** in ref 25c according to the Eyring theory. [f] Computed from equilibrium constant value of 32.7×10^{-1} of ref 25c. [g] B3PW91/UFF with P(*t*-Bu)$_3$ represented as PMe_3 at the QM level. [h] SDD quasirelativistic ECP and basis set augmented with polarization functions on P, Br, and Pd, 6-31G(d,p) on C and H. [i] Distances in Pd(*o*-Tolyl)Br(P(*t*-Bu)$_3$)/Pd(P(*t*-Bu)$_3$)$_2$. [j] Single point on BS I-optimized geometry with BS II: Martin's extended SDD basis set on Pd and Br, 6-311+G(2d,p) on C, H, P. [k] Single point on BS I-optimized geometry with BS III: Martin's extended SDD basis set on Pd and Br, AUG-cc-pVTZ on C, H, P. [l] Corrected for solvation with B3PW91/BS I single points on BS I optimized geometry with CPCM, a conductor-like screening model of C_6H_6 solvent. See experimental section for additional details of the computational methods.

deviations being potentially as significant for systems with agostic interactions,[29] and solvation contributions being important.

2. Ar−F Reductive Elimination from {Pd(Ar)F(NHC)}. Pd(Ph)F(Me$_2$NHC). Of the two common types of auxiliary ligands broadly able to support both Pd(II) and Pd(0) states in homogeneous catalysis—tertiary phosphines (PR_3) and *N*-heterocyclic carbenes (NHC)[1]—the former are susceptible to F^--mediated intramolecular oxidation by Pd(II), viz. P(III)/Pd(II)→P(V)/Pd(0), which yields fluorophosphines (R_2PF), fluorophosphoranes (R_2PF_3, R_3PF_2, R_4PF), and reductively coupled R−R, R_2P-PR_2 products together with reduced Pd.[30,21b,26e,g,h] Related to the other hard base-mediated oxidations of PR_3 by Pd(II),[31] the fluoride-induced redox reactivity renders even such deceptively ordinary complexes as $PdF_2(PR_3)_2$ stable only at or below 0 °C in solution.[32] Although tertiary phosphines successfully enable late transition metals catalysis of a wide variety of reactions that involve stoichiometric fluoride,[33] strong preference for P−F over C−F bond formation established for all known organometallic Pd(II) fluorides by Grushin suggests that auxiliary ligands other that PR_3 may need to be explored. While only a few M(NHC)F complexes have been characterized so far,[34a] NHC's could offer improved stability to intramolecular oxidation by Pd(II)/F^- in view of the potent fluorodehydroxylating reactivity of 2,2-difluoro-1,3-dimethylimidazolidine[34b] (a formal analog of a difluorophosphorane in such oxidation reaction), together with ability of NHC's to sustain otherwise harsh, oxidizing conditions of catalytic methane functionalization as supporting ligands for Pd.[34c] Following this reasoning and taking into account the greater intrinsic propensity of three- vs four-coordinate d^0 metal centers to undergo related C−X reductive eliminations,[35,25] Pd(Ph)F(Me$_2$NHC) became the initial focus of the computational study.

Reductive elimination of Ph−F from T-shaped Pd(Ph)F(Me$_2$NHC) (**1**) is computed to require $\Delta H^{\ddagger} = 28.9$ kcal/mol in the gas phase (**1**−**2**‡, Figure 1). Similar to the value in solution (C_6H_6, $\Delta H^{\ddagger} = 31.2$) as well as the $\Delta G^{\ddagger} = 29.8$, the enthalpy of **1**−**2**‡ implies a reaction time scale of hours at 100 °C. Partial IRC calculations (Supporting Information) confirmed Ph−F reductive elimination origin of **1**−**2**‡, although could not be extended to connect the reaction path from **1**−**2**‡ directly to either the metastable PhF−κF Pd^0 adduct **2** or another TS (**2**−**3**‡) with imaginary frequency normal mode depicting closely κF↔1,2η isomerization of PhF adducts **2** and **3**. These two stationary points, possibly traversed along the way from **1**−**2**‡

(29) These are limited to the structures optimized in the benchmark analysis, $_{PtBu_3}$**10**$_{NO_2}$ and $_{PtBu_3}$**10**−**11**$_{NO_2}{}^{\ddagger}$ (vide infra, Figure 9); in all other computed three-coordinate Pd(II) derivatives and transition states for reductive elimination of Ar-X auxiliary ligand hydrogens do not approach the metal closer than 2.7 Å. Cartesian coordinates and drawings with close contacts highlighted are provided in Supporting Information.

(30) (a) Mason, M. R.; Verkade, J. G. *Organometallics* **1990**, *9*, 864−865. (b) Mason, M. R.; Verkade, J. G. *Organometallics* **1992**, *11*, 2212−2220. (c) Marshall, W. J.; Grushin, V. V. *J. Am. Chem. Soc.* **2004**, *126*, 3068−3069. (d) Macgregor, S. A.; Roe, D. C.; Marshall, W. J.; Bloch, K. M.; Bakhmutov, V. I.; Grushin, V. V. *J. Am. Chem. Soc.* **2005**, *127*, 15304−15321.

(31) Grushin, V. V. *Chem. Rev.* **2004**, *104*, 1629−1662.

(32) (a) Yahav, A.; Goldberg, I.; Vigalok, A. *J. Am. Chem. Soc.* **2003**, *125*, 13634−13635. (b) Yahav, A.; Goldberg, I.; Vigalok, A. *Inorg. Chem.* **2005**, *44*, 1547−1553.

(33) For example, acting as a desilylating agent in Hiyama coupling[1c] and numerous other circumstances: Schwesinger, R.; Link, R.; Wenzl, P.; Kossek, S. *Chem.−Eur. J.* **2006**, *12*, 438−445.; as a base[1]; as a nucleofuge in cross-couplings with aryl fluorides: Kim, Y. M.; Yu, S. *J. Am. Chem. Soc*. **2003**, *125*, 1696−1697. Saeki, T.; Takashima, Y.; Tamao, K. *Synlett* **2005**, 1771−1774. Yoshikai, N.; Mashima, H.; Nakamura, E. *J. Am. Chem. Soc*. **2005**, *127*, 17978−17979. Bahmanyar, S.; Borer, B. C.; Kim, Y. M.; Kurtz, D. M.; Yu, S. *Org. Lett*. **2005**, *7*, 1011−1014. Terao, J.; Watabe, H.; Kambe, N. *J. Am. Chem. Soc*. **2005**, *127*, 3656−3657. Jasim, N. A.; Perutz, R. N.; Whitwood, A. C.; Braun, T.; Izundu, J.; Neumann, B.; Rothfeld, S.; Stammler, H.-G. *Organometallics* **2004**, *23*, 6140−6149. Braun, T.; Perutz, R. N. *Chem. Commun*. **2002**, 2749−2757.; or even as nucleophile in the original Tanaka's system (eq 1)[20].

(34) (a) Chatwin, S. L.; Davidson, M. G.; Doherty, C.; Donald, S. M.; Jazzar, R. F. R.; Macgregor, S. A.; McIntyre, G. J.; Mahon, M. F.; Whittlesey, M. K. *Organometallics* **2006**, *25*, 99−110. Schaub, T.; Radius, U. *Chem. Eur. J.* **2005**, *11*, 5024−5030. Laitar, D. S.; Müller, P.; Gray, T. G.; Sadighi, J. P. Organometallics **2005**, *24*, 4503−4505. (b) Hayashi, H.; Sonoda, H.; Fukumura, K.; Nagata, T. *Chem. Commun*. **2002**, 1618−1619. (c) Muehlhofer, M.; Strassner, T.; Herrmann, W. A. *Angew. Chem., Int. Ed*. **2002**, *41*, 1745−1747.

(35) (a) Tatsumi, K.; Hoffmann, R.; Yamamoto, A.; Stille, J. K. *Bull. Chem. Soc. Jpn*. **1981**, 1857−1867. (b) Morvskiy, A.; Stille, J. K. *J. Am. Chem. Soc*. **1981**, *103*, 4182−4186.(c) Driver, M. S.; Hartwig, J. F. *J. Am. Chem. Soc*. **1997**, *119*, 8232−8245.(d) Hartwig, J. F. *Acc. Chem. Res*. **1998**, *31*, 852−860.(e) Yamashita, M.; Hartwig, J. F. *J. Am. Chem. Soc*. **2004**, *126*, 5344−5345. (f) Hartwig, J. F. *Synlett* **2006**, 1283−1294.

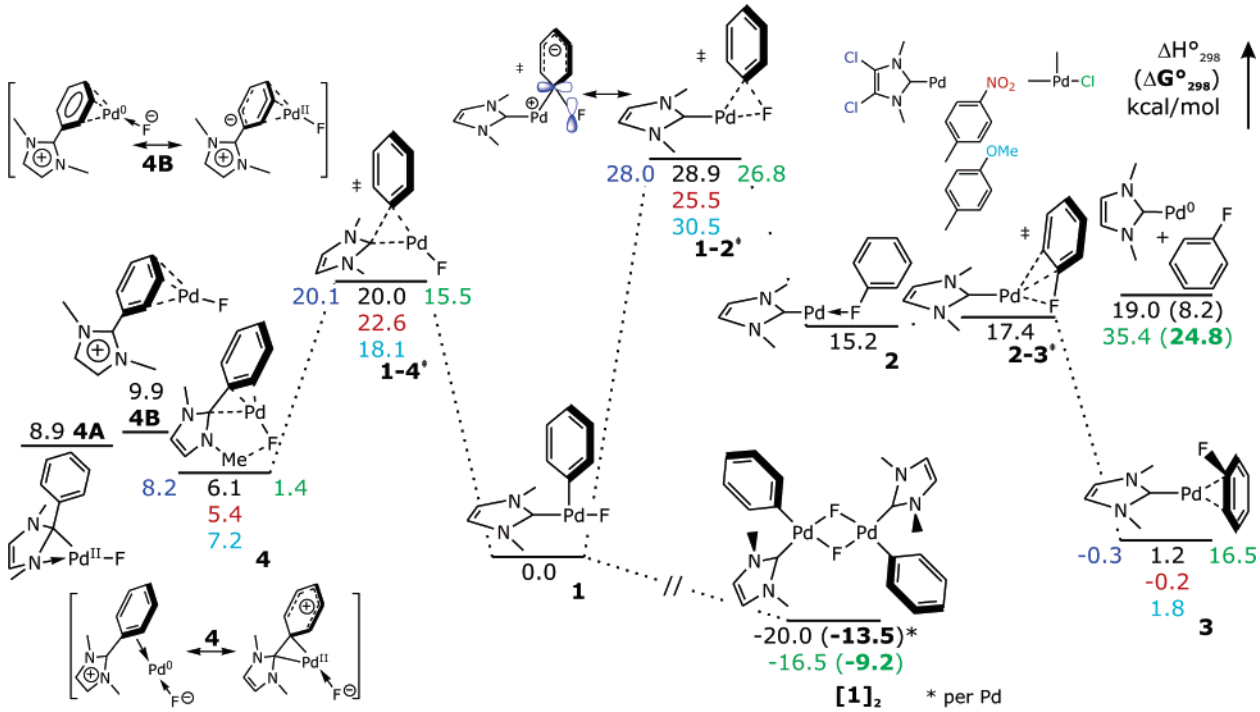

Figure 1. Computed reactivity profile of Pd(Ph)F(Me$_2$NHC) and related analogs: Pd(Ph)Cl(Me$_2$NHC) (numbers in green, right of center or below), Pd(Ph)F(4,5-Cl$_2$−Me$_2$NHC) (numbers in blue, left of center), Pd(C$_6$H$_4$-4-NO$_2$)F(Me$_2$NHC) (numbers in red, below center), and Pd(C$_6$H$_4$-4-OMe)F(Me$_2$NHC) (numbers in cyan, second below center).

to the global minimum Pd^0 product 1,2η-PhF adduct **3**, lie well below the reductive elimination TS **1**−**2**‡ (Figure 1) and would not be kinetically significant in the experimental practice. The final product of reductive elimination, **3**, is nearly isoenergetic with **1** ($\Delta H°$ = +1.2 kcal/mol) and lies 7.2 kcal/mol in $\Delta G°$ below the separated Pd^0(Me$_2$NHC) + PhF fragments. Thus, both kinetics and thermodynamics of Ph−F reductive elimination from a *three-coordinate* Pd(II) environment representative of those mediating closely related C−X bond forming reductive elimination processes[25,35] are computed to fall in a practical experimental range. Analogous elimination of Ph−Cl from $\mathbf{1}_{Cl}$ is characterized by $\Delta H^‡$ = 26.8 kcal/mol and $\Delta H°$ = +16.5 kcal/mol.[36] The substantial computed increase in the driving force for reductive elimination on going from Ph−Cl to Ph−F is largely attributable to Pd^{II}−X BDE ($\Delta H°_{Pd-X\rightarrow Pd\bullet+X\bullet}$, $\mathbf{1}_{Cl}$: 89.5; **1**: 103.3 kcal/mol) lagging behind that of Ph−X (Cl: 93.3, F: 123.4 kcal/mol) on going to lighter halides. Given the demonstrated precedent of reductive elimination of heavy aryl halides from Pd(II),[25a,c,d] the magnitude of the computed driving force increase on going to F offers a promising outlook for thermodynamics of such Ar−F bond forming reactions.

However, **1** would be considerably more prone to elimination of phenyl-imidazolium ion, transition state for which (**1**−**4**‡) is computed to lie 8.8 kcal/mol below that for Ph−F reductive elimination (**1**−**2**‡). Extensively studied experimentally and computationally by Cavell and Yates, such intramolecular migratory processes resulting in transfer of hydrocarbyl ligands to NHC carbon are now well-known to limit the usefulness of NHC's as supporting ligands to relatively facile productive reactions of M(R)(NHC) intermediates.[37] Three isomeric forms of the Ph−NHC migration product were located in the case of **4** within 3.8 kcal/mol of each other, with one (**4A**) clearly maintaining Pd(II) oxidation state in a distorted Y-shaped geometry and the others (**4** and **4B**) best described by mixed Pd^0↔Pd^{II} zwitter-ionic resonance forms also shown in Figure 1.[38] Although the reaction of **1** rate-limited by **1**−**4**‡ is endothermic by 6.1 kcal/mol (**4**) and thus may exhibit at least some degree of reversibility, irreversible decomposition by loss of Ph−NHCMe$_2^+$ from **4** and aggregation to Pd black is likely to be facile enough to preclude **1** from undergoing Ph−F reductive elimination altogether.

Most importantly, the very existence of three-coordinate **1** in solution requires $\Delta G°$ = 13.5 kcal/mol (per monomer) relative to the fluoride-bridged dimer form **[1]**$_2$ (Figure 1). Inclusion of this uphill pre-equilibrium into consideration places $\Delta G^‡$ for Ph−F reductive elimination chiefly out of practical experimental range, at 13.5 + 29.8 = 43.3 kcal/mol for a rapid pre-equilibrium dissociation of **[1]**$_2$ followed by rate-limiting elimination from **1** via TS **1**−**2**‡ (complete dimer cleavage could

(36) $\Delta G^‡(C_6H_6)$ = 10.6 kcal/mol for the reverse process, oxidative addition of PhCl in $\mathbf{3}_{Cl}$, compares well with the value of 9.4 kcal/mol obtained for this process in a different computational study: Green, J. C.; Herbert, B. J.; Lonsdale, R. *J. Organomet. Chem*. **2005**, *690*, 6054−6067.

(37) (a) McGuinness, D. S.; Green, M. J.; Cavell, K. J.; Skelton, B. W.; White, A. H. *J. Organomet. Chem.* **1998**, *565*, 165−178. (b) McGuinness, D. S.; Cavell, K. J.; Skelton, B. W.; White, A. H. *Organometallics* **1999**, *18*, 1596−1605. (c) McGuinness, D. S.; Saendig, N.; Yates, B. F.; Cavell, K. J. *J. Am. Chem. Soc*. **2001**, *123*, 4029−4040. (d) Nielsen, D. J.; Magill, A. M.; Yates, B. F.; Cavell, K. J.; Skelton, B. W.; White, A. H. *Chem. Commun*. **2002**, 2500−2501. (e) Caddick, S.; Cloke, F. G. N.; Hitchcock, P. B.; Leonard, J.; Lewis, A. K. de K.; McKerrecher, D.; Titcomb, L. R. *Organometallics* **2002**, *21*, 4318−4319. (f) Lewis, A. K. de K.; Caddick, S.; Cloke, F. G. N.; Billingham, N. C.; Hitchcock, P. B.; Leonard J. J. *Am. Chem. Soc*. **2003**, *125*, 10066−10073. (g) Marshall, W. J.; Grushin, V. V. *Organometallics* **2003**, *22*, 1591−1593. (h) Crudden, C. M.; Allen, D. P. *Coord. Chem. Rev.* **2004**, *248*, 2247−2273. (i) Cavell, K. J.; McGuinness, D. S. *Coord. Chem. Rev.* **2004**, *248*, 671−681. (j) Graham, D. C.; Cavell, K. J.; Yates, B. F. *Dalton Trans*. **2005**, 1093−1100. (k) Graham, D. C.; Cavell, K. J.; Yates, B. F. *Dalton Trans*. **2006**, 1768−1775.

(38) Contributing resonance forms have been identified on the basis of computed geometrical parameters only, available in Supporting Information. Mixed resonance form assignments do not bear any quantitative connotation.

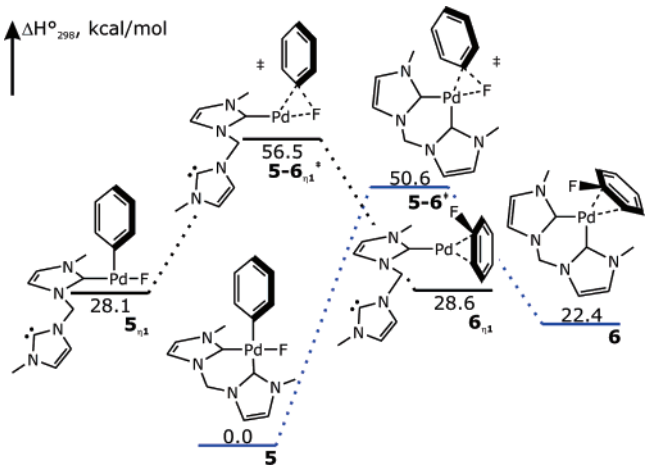

Figure 2. Computed effects of coordination of an additional strong donor ligand on Ph−F reductive elimination from a three-coordinate PdPh(F)L.

require even greater activation, vide infra). At the same time, **[1]**$_2$ may still suffer reductive elimination of Ph−NHCMe$_2^+$, either via **1** and TS **1**−**4**‡ or directly from saturated **[1]**$_2$, given such precedent for at least the alkyl-NHC eliminations from neutral four-coordinate d^8 metal complexes.[37c] Thus, it appears that any potential benefit of improved stability to intramolecular oxidation by Pd(II)/F$^-$ offered by NHC's in comparison to phosphines would be undermined by susceptibility of the former to reductive elimination with the hydrocarbyl group, at least as long as the $\Delta H^‡$ for Ph−F reductive elimination remains noncompetitive.

Pd(Ph)F((MeNHC)$_2$CH$_2$). A productive strategy to inhibit hydrocarbyl-NHC reductive elimination from d^8 metal complexes is to incorporate the NHC ligand in a multidentate assembly that resists rotation of the NHC ring out of the coordination plane, into an orientation adequately suited for formation of partial bonding between the eliminating fragments (cf. **1**−**4**‡).[37d,i] Seeking to assess the utility of this approach with the chelating bis-carbene ligand (MeNHC)$_2$CH$_2$ in the computational model **5** (Figure 2) showed instead a remarkably profound effect of coordinative saturation on the kinetics of Ph−F reductive elimination from Pd(II).

Coordination of the second arm of the chelating bis-carbene ligand to Pd, while favorable for all stationary points on the elimination pathway, stabilizes the oxidized Pd^{II} state (**5**$_{\eta 1}$) by nearly 22 kcal/mol more than it does both the elimination transition state **5**−**6**$_{\eta 1}^‡$ and the Pd^0 product **6**$_{\eta 1}$. The relative stabilization of the Pd^{II} reactant raises the magnitude of the Ph−F reductive elimination $\Delta H^‡$ to 50.6 kcal/mol (**5**−**6**‡), or well outside of the realm of synthetically relevant values. Considered in reverse, increase of the elimination driving force by destabilization of the saturated reactant **5** via ligand loss is invaluable in translating into a substantial decrease of the activation enthalpy.

Substituent Effects. Kinetics of aryl-fluoride reductive elimination from Pd(C$_6$H$_4$-*p*-X)F(Me$_2$NHC) models **1**$_{OMe}$, **1**, **1**$_{NO_2}$ show substantial improvement with increasingly electron-withdrawing para-substituents on the aryl ring (Figure 1). Closely reminiscent of the experimental findings on related C−S,[39a,b] C−N,[35c] and C−O[24c,f] reductive eliminations, computational C−F data in Figure 1 show this to be primarily a stabilizing TS effect ($\Delta\Delta H^‡ = -5.0$ kcal/mol), with analogous but smaller influence on the driving force ($\Delta\Delta H° = -2.1$ kcal/mol). Like the related polar carbon−heteroatom reductive eliminations,[35d,f] and to a greater extent nucleophilic aromatic substitutions,[7] elimination of Ar−F from Pd^{II} is promoted by electron-withdrawing para-substituents of the aryl group, primarily in kinetics. On the contrary, reductive elimination of Ar−NHC$^+$ from **1**$_{OMe}$-**1**$_{NO_2}$ is inhibited by electron-withdrawing *p*-Ar substituents ($\Delta\Delta H^‡ = +4.5$ kcal/mol), signifying importance of a dative interaction between the filled Ar σ orbital and NHC π^* to the bonding in the TS **1**−**4**‡. To an extent, Ar−NHC$^+$ elimination from **1** is initiated by a nucleophilic attack of the Ar at the NHC C-2.[37k] Thermodynamics of Ar−NHC$^+$ elimination (**4**) vary in the opposite direction from kinetics (**1**−**4**‡) in the same series **1**$_{OMe}$−**1**$_{NO_2}$ ($\Delta\Delta H° = -1.8$ kcal/mol) apparently reflecting the dominant contribution of the Pd^0 resonance form, whose stability is indeed enhanced by stronger π-acidity of the π-bound 1,2η-C$_6$H$_4$-4-X aryl ring, to the structure of **4**. Because characteristics of the aryl groups that promote Ar−F (**1**−**2**‡, electrophilic) and Ar−NHC$^+$ (**1**−**4**‡, nucleophilic) reductive eliminations from **1** are opposite of each other, variation of para-substituent from OMe to NO$_2$ causes a pronounced reduction in the relative preference for (X-4-C$_6$H$_4$)-NHC$^+$ elimination over that of (X-4-C$_6$H$_4$)−F, from 12.4 to 2.9 kcal/mol in $\Delta\Delta H^‡$. Thus, Ar−F elimination may be able to out compete decomposition of PdAr(F)(NHC) via Ar−NHC$^+$ elimination with electron-deficient Ar.

Replacement of Me$_2$NHC with electron-deficient 4,5-dichloro Me$_2$NHC in **$_{Cl2}$1** promotes kinetics of Ph−F reductive elimination ($\Delta\Delta H = -0.8$ kcal/mol) in accord with Hammond postulate ($\Delta\Delta H° = -1.6$ kcal/mol) and exerts nearly opposing influence on kinetics (**$_{Cl2}$1**−**4**‡, $\Delta\Delta H^‡$0.0) and thermodynamics (**$_{Cl2}$4**, $\Delta\Delta H° = +2.1$) of Ph−NHC$^+$ reductive elimination, as expected for the latter process starting out as a nucleophilic attack of Ar at C-2 (**$_{Cl2}$1**−**4**‡, cf. **1**−**4**$_{OMe}^‡$, **1**−**4**$_{NO_2}^‡$, vide supra), but resulting in a net increase of positive charge on the NHC ring in the product (**$_{Cl2}$4**).

The Role of F$^-$. Increasing electrophilicity of either Pd (**1**−**2**‡ vs **$_{Cl2}$1**−**2**‡) or the aryl (**1**−**2**$_{OMe}^‡$ vs **1**−**2**$_{NO_2}^‡$) causes relative stabilization of **1**−**2**‡ as the Ar−F bond-making transition state. Could the difficulty of making the C−F bond from **1** via **1**−**2**‡ reflect localization of excessive negative charge on F$^-$ in the TS[40] and may the process be facilitated by binding an external electrophile directly to F$^-$? To assess these hypotheses, an HF molecule was added to the Pd(Ph)F(Me$_2$NHC) model **1** as a hydrogen-bond donor to the F$^-$ ligand. Although it was possible to fully optimize transition state **1**−**2**$_{...HF}^‡$ with HF bound almost solely via the (Pd)F···HF hydrogen bond, energies of the purely (F)H···F(Pd) hydrogen-bonded HF adducts **1**$_{...HF}$ and **3**$_{...HF}$ were obtained as upper estimates from incomplete optimizations due to their respective instabilities to **1**$_{-HF}$ and **3**$_{-HF}$ (Figure 3). The comparative electronic energy profile that emerged resembles that of the bi-/monodentate (MeNHC)$_2$CH$_2$ models **5**, **5**$_{\eta 1}$ (Figure 2): like coordination of the additional ligand to Pd, formation of a hydrogen bond to F$^-$ undergoing Ph−F reductive elimination serves mostly to stabilize Pd^{II} reactant **1**, reducing the driving force ($\Delta\Delta E° = 12.1$ kcal/mol) and raising the activation

(39) (a) Barañano, D.; Hartwig, J. F. *J. Am. Chem. Soc.* **1995**, *117*, 2937−2938. (b) Mann, G.; Barañano, D.; Hartwig, J. F.; Rheingold, A. L.; Guzei, I. A. *J. Am. Chem. Soc.* **1998**, *120*, 9205−9219. (c) Mann, G.; Hartwig, J. F.; Driver, M. S.; Fernández-Rivas, C. *J. Am. Chem. Soc.* **1998**, *120*, 827−828.

(40) Seppelt, K. *Angew. Chem., Int. Ed. Engl.* **1992**, *31*, 292−293.

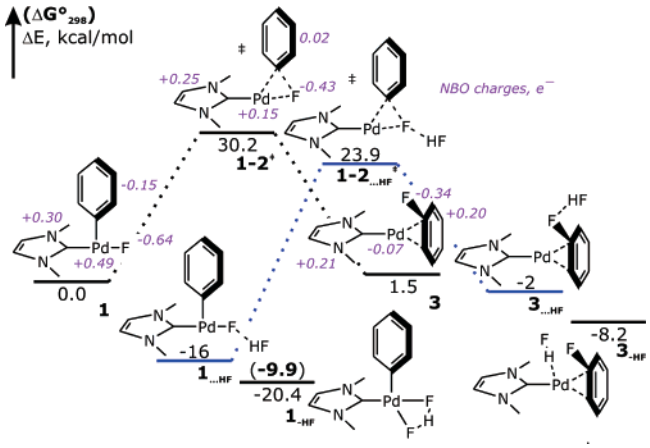

Figure 3. Computed effects of formation of hydrogen bonds between F and external HF on Ph−F reductive elimination from Pd(Ph)F(Me$_2$NHC)L.

barrier ($\Delta\Delta E^{\ddagger} = 9.5$ kcal/mol) comparably and considerably. This result is not surprising in view of the NBO fragment charges also shown in Figure 3, which reveal a monotonic decrease of the F$^-$ value on going from **1** (−0.64) to **1**−**2**‡ (−0.43) to **3** (−0.34 e$^-$). Thus, the fluoride becomes progressively less "naked" during Ph−F reductive elimination, and although TS **1**−**2**‡ does benefit from hydrogen bonding to F$^-$ in absolute terms, reactant **1** with a more basic F$^-$ does so much more, leading to a net increase of the activation barrier on going from **1** to **1**$_{...HF}$.

Promotion of Ar−F reductive elimination from PdArF(L) by more weakly donating auxiliary L can therefore be safely attributed to destabilization of oxidized **1**, featuring largest positive charge on Pd (Figure 3), relative to Pd^0 elimination product **3** and less so TS **1**−**2**‡. Recurrent throughout calculations (vide infra), this trend follows the textbook axiom of reductive elimination being stimulated by increasing positive charge at the metal,[41] such as by reducing auxiliary ligand donor strength, or indeed their number (Figure 2). With partial positive charge on the metal decreasing monotonically during the reductive elimination (Figure 3), driving force is affected the most by such auxiliary ligand variation, with a smaller promoting influence also exerted on the elimination TS, producing accord with the Hammond postulate. As the aryl ligand does not remain auxiliary during elimination, thermodynamic effects of aryl substituents are less transparent. However, clear structural resemblance to a Meisenheimer intermediate born by TS **1**−**2**‡ (in its cyclohexadienyl resonance form shown in Figure 1), shows that any electronic effects of Ar substituents promoting S$_N$Ar reactivity[7] will be operative in Ar−F reductive elimination as well. Therefore, significant stabilization of TS **1**−**2**‡ by *para* electron-withdrawing groups on Ar (**1**−**2**$_{\mathbf{OMe}}^{\ddagger}$ vs **1**−**2**$_{\mathbf{NO_2}}^{\ddagger}$) relative to both **1** and **3** can be at least partly attributed to an S$_N$Ar reaction character of the Ar−F reductive elimination (and oxidative addition[42]). Thus to some extent, F$^-$ acts as a nucleophile/nucleofuge with respect to the Ar in these reactions

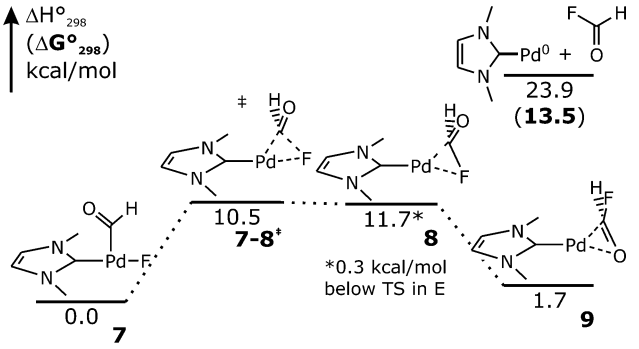

Figure 4. Computed HC(O)−F reductive elimination reactivity profile of Pd(C(O)H)F(Me$_2$NHC).

and dative F$^-$(p)→Ar(π*) interactions,[43] promoted by para electron-withdrawing substituents on Ar, comprise an important contribution to the bonding in TS **1**−**2**‡. Notably, structural differences between **1**−**2**$_{\mathbf{OMe}}^{\ddagger}$ and **1**−**2**$_{\mathbf{NO_2}}^{\ddagger}$ accompanying the −5.0 kcal/mol difference in their $\Delta H^{\ddagger}$ amount only to a 0.05 Å shorter Pd···Ar distance and a 2° sharper angle at F in **1**−**2**$_{\mathbf{NO_2}}^{\ddagger}$.

Aspects of S$_N$Ar have been thoroughly recognized in the experimental mechanistic studies of related (aromatic) C−S,[39a,b] C−N,[35c] and C−O[24c,f] reductive eliminations from Pd^{II}. For all of these reaction categories, elimination kinetics were found to correlate strongly with nucleophilicity of the heteroatom-containing group,[35f,39c] further corroborating the mechanistic analogy based on aryl substituent effects. The importance of the X group nucleophilicity to C−X reductive elimination kinetics is striking, for example, in being responsible for considerably faster rates of C−S bond-forming reactions in comparison to the more thermodynamically favorable C−N and C−O eliminations.[35f] Conversely, kinetic challenges facing C−F reductive elimination in experimental practice may be attributed to poor nucleophilicity of Pd^{II}-bound F$^-$—very different from a "naked" F$^-$ form[40]—extrapolating the rationale put forth for the kinetic order of heavy aryl-halide reductive eliminations from Pd^{II}.[25c] Thus, it may appear as no surprise that hydrogen bonding, reducing nucleophilicity of Pd-bound F$^-$ in **1**−**2**‡ further, is detrimental to the elimination kinetics (Figure 3). However, this net kinetic effect can be attributed entirely to greater relative stabilization of reactant **1** with its more basic F$^-$. A substrate more susceptible to nucleophilic attack was therefore considered to reveal more clearly any potential kinetic benefits of promoting dative F$^-$→C interactions between eliminating fragments in the TS. Indeed, Figure 4 shows how dramatically more reactive a formyl group is compared to Ph, to C(sp^2)−F reductive elimination from the three-coordinate Pd^{II} environment of **7**. A computed $\Delta\Delta H^{\ddagger}$ reduction of 18.4 kcal/mol on going from **1**−**2**‡ to **7**−**8**‡ is accompanied by a slight decrease in reaction driving force ($\Delta\Delta H^{\circ} = +0.4$ kcal/mol)[44] with respect to the most stable Pd^0 adduct of the reductively coupled R−F in each case, **3** and **9**, and can thus be attributed chiefly to the presence of a more accessible acceptor orbital ($\pi^*_{C=O}$) on the sp^2 carbon of R in **7**. This comparison demonstrates a clear advantage to the kinetics of C−F reductive

(41) Collman, J. P.; Hegedus, L. S.; Norton, J. R.; Finke, R. G. *Principles and Applications of Organotransition Metal Chemistry*, 2nd ed.; University Science Books: Mill Valley, CA, 1987; pp 322−333.
(42) Oxidative addition of heavy aryl halides to [Pd^0(PP)] *in THF solvent* was computed to proceed via classical S$_N$Ar mechanism followed by collapse of the resulting ion pair: Senn, H. M.; Ziegler, T. *Organometallics* **2004**, *23*, 2980−2988.
(43) Represented schematically in the cyclohexadienyl resonance form of TS **1**−**2**‡ in Figure 1 and illustrated in two canonical MO isosurfaces computed for **1**−**2**$_{\mathbf{NO_2}}^{\ddagger}$ (Supporting Information); for a recent computational analysis of orbital interactions in transition states for C−X oxidative addition to Pd(0)L$_n$, see: Ariafard, A.; Lin, Z. *Organometallics* **2006**, *25*, 4030−4033.
(44) This thermodynamic invariance is consistent with similarity of BDE's[10] of HC(O)−F (119) and Ph−F (126 kcal/mol).

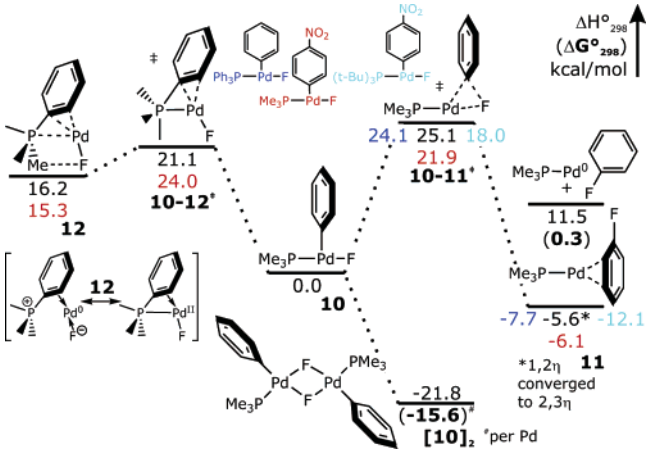

Figure 5. Computed reactivity profile of Pd(Ph)F(PMe_3) and related analogs: Pd(C_6H_4-4-NO_2)F(P(*t*-Bu)$_3$) (numbers in cyan, right of center), Pd(Ph)F(PPh_3) (numbers in blue, left of center), and Pd(C_6H_4-4-NO_2)F(PMe_3) (numbers in red, below center).

elimination/oxidative addition of dative $F^-(p)\rightarrow C(\pi^*)$ σ-symmetry interactions between eliminating fragments,[43] a secondary bonding mode geometrically constrained to be most favorable in the TS of concerted processes. Calculations also suggest that C−F reductive elimination from Pd^{II} can in principle operate in a very fast kinetic regime (of synthetic applications), and support the notion of ArC(O)−F reductive elimination from Pd^{II} indeed mediating the carbonylative halide exchange fluorination (fluorocarbonylation) of aryl halides (eq 1).[20,21]

3. Ar−F Reductive Elimination from {Pd(Ar)F(PR3)}. Figure 5 shows many of the trends computed for Ar−F reductive elimination from Pd(Ar)F(NHC) in Figures 1−3 persisting in the phosphine-supported Pd^{II} environment. Thus, the PMe_3 analog of **1**, Pd(Ph)F(PMe_3) (**10**), is predicted to be well suited for reductive elimination of Ph−F ($\Delta H^{\ddagger} = 25.1$, $\Delta H^{\circ} = -5.6$ kcal/mol), and even greater reactivity should be expected of its three-coordinate PPh_3 derivative ($\Delta H^{\ddagger} = 24.1$, $\Delta H^{\circ} = -7.7$ kcal/mol). Consideration of the respective Ph−F elimination $\Delta H^{\ddagger}$ (ΔH°) of 28.9 (+1.2) and 28.0 (−0.3) kcal/mol characterizing such reactivity of **1** and $_{Cl2}$**1** suggests both NHC ligands to be better donors to Pd^{II} in **1** than PMe_3. The decreasing donor ability in the auxiliary ligand series **1**, $_{Cl2}$**1**, **10**, $_{PPh_3}$**10** results in lowering of activation enthalpy by the total of $\Delta\Delta H^{\ddagger} = -4.0$ kcal/mol and proportionally greater increase in the driving force, $\Delta\Delta H^{\circ} = -8.9$ kcal/mol, in accord with the Hammond postulate and the basic arguments of decreasing positive charge at the metal accompanying reductive elimination (vide supra). Also consistent with Pd(Ar)F(NHC) results, substitution of the aryl ring of **10** with electron-withdrawing *p*-NO_2 promotes reductive elimination with a sizable S_NAr-type kinetic effect ($\Delta\Delta H^{\ddagger} = -3.2$, $\Delta\Delta H^{\circ} = -0.5$ kcal/mol).

PdAr(F)L(PR_3). Increasing electrophilicity of Pd on going from **1** to **10**, while promoting Ph−F reductive elimination, also stabilizes the fluoride-bridged dimer form $[\mathbf{10}]_2$, by $\Delta\Delta H^{\circ} = -1.9$ kcal/mol per monomer relative to $\mathbf{1}\rightarrow 1/2[\mathbf{1}]_2$ (Figures 1, 5). Like $[\mathbf{1}]_2$, $[\mathbf{10}]_2$ would be unable to undergo Ph−F reductive elimination via rapid pre-equilibrium breakup to **10** followed by rate-limiting **10**−**11**‡, with the added dimer dissociation $1/2\Delta G^{\circ}$ raising the $\Delta G_{obs}^{\ddagger}$ from that of **10**−**11**‡ to 25.5 + 15.6 = 41.1 kcal/mol (cf. 43.3 for $[\mathbf{10}]_2$; both are lower estimates with dimer dissociation not being rate-limiting, vide infra), an activation barrier again too high for practical synthetic applications. Coordination of another PMe_3 to **1** ($\Delta H^{\circ} = -25.5$, $\Delta G^{\circ} = -12.9$ kcal/mol) is favorable by ∼12 kcal/mol more than that to **10**−**11**‡ and **11**, with the difference translating directly into lowered driving force ($\Delta H^{\circ} = +5.1$ kcal/mol) and increased activation barrier ($\Delta H^{\ddagger} = 38.8$ kcal/mol) for Ph−F reductive elimination from **13** (Figure 6) compared to that from **10**. Although together with comparative reactivity of **5** and $\mathbf{5}_{\eta 1}$ (Figure 2) this result speaks against the utility of four-coordinate Pd^{II} environment for mediating Ar−F reductive elimination, coordination of I^- to $_{PPh_3}$**10** produces a notable exception. Palladate **15** is computed to undergo Ph−F reductive elimination with $\Delta H^{\ddagger} = 26.4$ kcal/mol in the gas phase, a barrier of only 2.3 kcal/mol higher than that computed for $_{PPh_3}$**10** (Figure 6).[45] This finding is particularly encouraging in view of the appreciable stability of the heavy halide analogs of **15**, [Cat][Pd(Ph)X_2(PPh_3)] (X = Cl, Br, I) relative to dimers [Pd(Ph)PPh_3(μ-X)]$_2$ and [Cat]X in CD_2Cl_2 determined experimentally.[26e] However, it is also notable that analogous [Pd(Ar)(pyrrolyl)$_2$L]$^-$ palladates were found less reactive toward *N*-aryl pyrrole reductive elimination than their neutral [Pd(Ar)(pyrrolyl)L_2] derivatives.[39c]

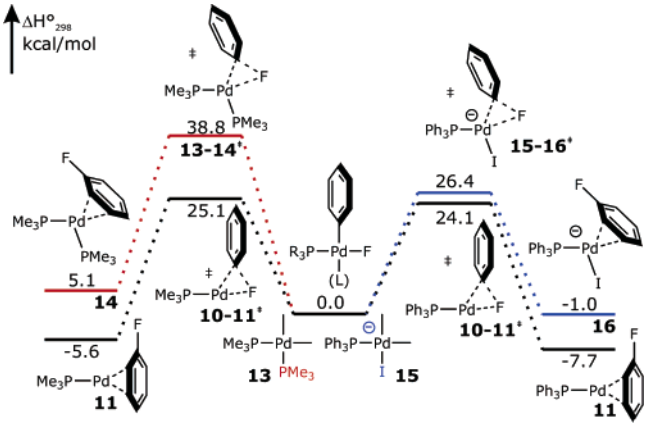

Figure 6. Computed effects of coordination of additional donor ligands on Ph−F reductive elimination from three-coordinate PdPh(F)PR_3.

P(III)/Pd(II)→P(V)/Pd(0). Intramolecular oxidation of phosphines by Pd(II)/F^- has been identified experimentally as the key process competing with Ar−F reductive elimination from [Pd^{II}](Ar)F(PR_3) complexes (vide supra).[21b,26e,g,h] Although recent studies provided compelling evidence for formation of fluorophosphines R_2PF by intramolecular R_2P−R/M−F exchange,[30c,d] supporting their proposed intermediacy in the overall decomposition process,[26e] complete mechanistic picture remains tentative. To evaluate the feasibility of Ar−F reductive elimination from three-coordinate Pd(Ar)F(PR_3) in comparison to intramolecular PR_3 oxidation by Pd(II)/F^-, yet another decomposition process was considered as a benchmark. Thermolysis of Pd(Ph)F(PPh_3)$_2$ showed the onset temperature of reversible Ph−Ph/Pd−Ph exchange to be detectably lower than that of irreversible PR_3 oxidation by Pd(II)/F^-.[26e] Evaluation of the barrier to the former process, generally accepted to proceed via reductive elimination of aryl-phosphonium ion and accelerated

(45) Activation enthalpies of both $_{PPh_3}$**10**−**11**‡ and **15**−**16**‡ increase by ∼3 kcal/mol each in C_6H_6 with net, favorable solvation energy being ∼20 kcal/mol greater for the anionic derivatives.

by ligand dissociation from square-planar precursors,[46] could thus serve as an approximate (lower bound) measure of the $R_3P-Pd(II)/F^-$ oxidation kinetics.

Figure 5 shows migration of Ph from Pd in **10** to coordinated PMe_3 to face a kinetic barrier (**10**−**12**‡, $\Delta H^{\ddagger} = 21.1$ kcal/mol, see also Supporting Information) considerably lower than that of reductive elimination of Ph−F (**10**−**11**‡, $\Delta H^{\ddagger} = 25.1$ kcal/mol). The Ph−PMe_3 coupled product **12**, decidedly unstable with respect to **10** ($\Delta H^{\circ} = +16.2$ kcal/mol), adopts a gas-phase structure best described by a combination of resonance forms of 1,2η-$C_6H_5-PMe_3^+$ adduct of $Pd^0(F^-)$ and Pd^{II} phosphoranide Pd(PPhMe$_3$)F, featuring short Pd−P (2.31 Å, cf. 2.25 Å in **10**) and Pd···C1,C2 (2.10, 2.30 Å) distances.[38] Presence of electron-withdrawing *p*-NO_2 on the migrating phenyl group in **10**−**12**‡ raises the barrier by $\Delta\Delta H^{\ddagger} = 2.9$ kcal/mol, consistent with experimental trends,[46d] and stabilizes the Ar−PMe_3 coupled structure by $\Delta\Delta H^{\circ} = 0.9$ kcal/mol. As a result of the opposite substituent effect *p*-NO_2 group has on the Ph−F elimination kinetics, latter reaction becomes more facile than PMe_3 arylation ($\Delta\Delta H^{\ddagger} = -2.1$ kcal/mol) for $\mathbf{10}_{\mathbf{NO_2}}$. All changes resulting from *p*-NO_2 substitution in **10** duplicate substituent effects in **1** (Figure 1). Thus, subject to the validity of the above assumption of the relative activation barriers of P−C and P−F bond-forming decomposition processes in a three-coordinate $[Pd^{II}](Ar)F(PR_3)$ environment, computational results in Figure 5 suggest that Ar−F reductive elimination may be able to compete with irreversible oxidation of PR_3 by $Pd(II)/F^-$, with improved selectivity for C−F bond formation displayed by more electron-deficient Ar substrates.

Steric Factors. The key advantage of the $[Pd^{II}](Ar)F(PR_3)$ environment in practice over that based on NHC's is the availability of a series of sterically demanding PR_3 ligands, whose bulk may serve to additionally facilitate C−F reductive elimination process. The series of Pd(Ar)X(P(*t*-Bu)$_3$) complexes investigated by Hartwig, in particular, exemplify such remarkable effects of bulky and strongly electron-donating phosphines, both in the stability of the unique 14-electron complexes with weak agostic interactions and their unprecedented reactivity by reductive elimination of heavy aryl halides.[25,35e] Computational data in Figure 5 reveal the magnitude of steric effects on elimination barrier that might be accessible in the case of Pd(Ar)F(P(*t*-Bu)$_3$): reductive elimination of $(O_2N\text{-}4\text{-}C_6H_4)-F$ from $_{\mathbf{PtBu_3}}\mathbf{10}_{\mathbf{NO_2}}$, evaluated with ONIOM models, requires $\Delta H^{\ddagger}$ 3.9 kcal/mol lower than that from its PMe_3 analog $\mathbf{10}_{\mathbf{NO_2}}$ and is subject to a 6.0 kcal/mol greater driving force, although each change is likely overestimated in comparison to experiment due to poor representation of CH···Pd agostic interactions in both $_{\mathbf{PtBu_3}}\mathbf{10}_{\mathbf{NO_2}}$ and $_{\mathbf{PtBu_3}}\mathbf{10}-\mathbf{11}_{\mathbf{NO_2}}^{\ddagger}$ (vide supra).[29]

Collectively, computational studies show that auxiliary ligands of high steric demand but moderate donor strength, together with electron-poor aryl substrates, create the most promising environment for Ar−F reductive elimination from three-coordinate Pd^{II}.

B. Experimental Studies. 1. Synthesis of [Pd(C$_6$H$_4$-4-NO$_2$)L(μ-F)]$_2$, L = P(*o*-Tolyl)$_3$, P(*t*-Bu)$_3$. Following the insight gained from computational studies, the novel $[Pd(C_6H_4\text{-}4\text{-}NO_2)L(\mu\text{-}F)]_2$ featuring sterically demanding L = P(*o*-Tolyl)$_3$ (**17**) and P(*t*-Bu)$_3$ (**18**) were prepared starting from the known[47] $[Pd(C_6H_4\text{-}4\text{-}NO_2)P(o\text{-Tolyl})_3(\mu\text{-I})]_2$ (Scheme 1), isolated and fully characterized. We found AgF metathesis[21] of the Pd iodide precursor to require sonication over simple stirring,[32] but also a catalytic amount of P(*o*-Tolyl)$_3$. Both **17** and **18** maintain fluoride-bridged dimer structures in solution, even at elevated temperatures (vide infra). Stability of dimeric $[PdArL(\mu\text{-}F)]_2$ ground states with L of the largest cone angles characterized so far in a {Pd}F coordination environment contrasts with the structural preferences of the X = Br and I analogs of P(*t*-Bu)$_3$ derivative **18**[25], although does follow the trend of related Pd(Ar)X(Q-Phos) that adopt dimeric structure with X = Cl but not Br or I.[47b]

Scheme 1. Synthesis and Solution Characterization of **17** and **18**

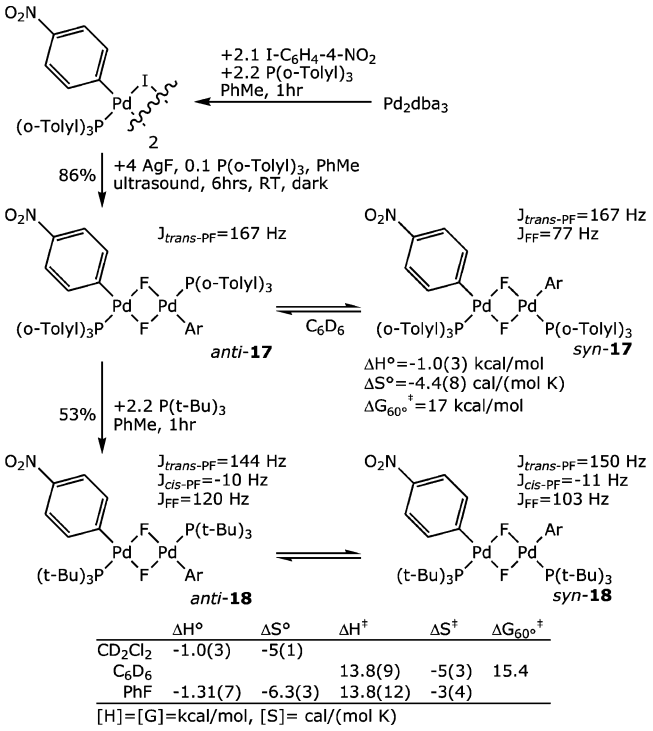

	ΔH°	ΔS°	ΔH‡	ΔS‡	ΔG$_{60°}$‡
CD_2Cl_2	-1.0(3)	-5(1)			
C_6D_6			13.8(9)	-5(3)	15.4
PhF	-1.31(7)	-6.3(3)	13.8(12)	-3(4)	

[H]=[G]=kcal/mol, [S]= cal/(mol K)

Solution Structures. Variable-temperature NMR studies of **17** and **18** in several solvents revealed existence of interconverting *syn* and *anti* isomeric forms of the dimers and allowed measurement of individual spectroscopic data, while iterative line shape analysis[48] enabled determination of thermodynamic and activation parameters governing the *anti*↔*syn* equilibrium in each complex. Scheme 1 summarizes these data, and Figure 7 shows representative of the observed and fitted NMR lineshapes (complete results can be found in Supporting Information).

For both **17** and **18** isomerization of *anti* to *syn* form is marginally exothermic ($\Delta H^{\circ} = -1$ kcal/mol), with *anti*↔*syn* equilibrium ΔS° sufficiently negative (−5 cal/(mol K)) to render *syn* form the minor isomer in all but one spectra obtained, diminishing in equilibrium concentration with increasing temperature. Increasing solvent polarity shifts *anti*↔*syn* equilibrium

(46) (a) Kong, K.-C.; Cheng, C.-H. *J. Am. Chem. Soc.* **1991**, *113*, 6313−6315. (b) Segelstein, B. E.; Butler, T. W.; Chenard, B. L. *J. Org. Chem.* **1995**, *60*, 12−13. (c) Morita, D. K.; Stille, J. K.; Norton, J. R. *J. Am. Chem. Soc.* **1995**, *117*, 8576−8581. (d) Goodson, F. E.; Wallow, T. I.; Novak, B. M. *J. Am. Chem. Soc.* **1997**, *119*, 12441.

(47) (a) Paul, F.; Patt, J.; Hartwig, J. F. *Organometallics* **1995**, *14*, 3030−3039. (b) Barrios-Landeros, F.; Hartwig, J. F. *J. Am. Chem. Soc.* **2005**, *127*, 6944−6945.

(48) Budzelaar, P. H. M. *gNMR*, version 5.0.6.0; IvorySoft: Englewood, CO, 2006.

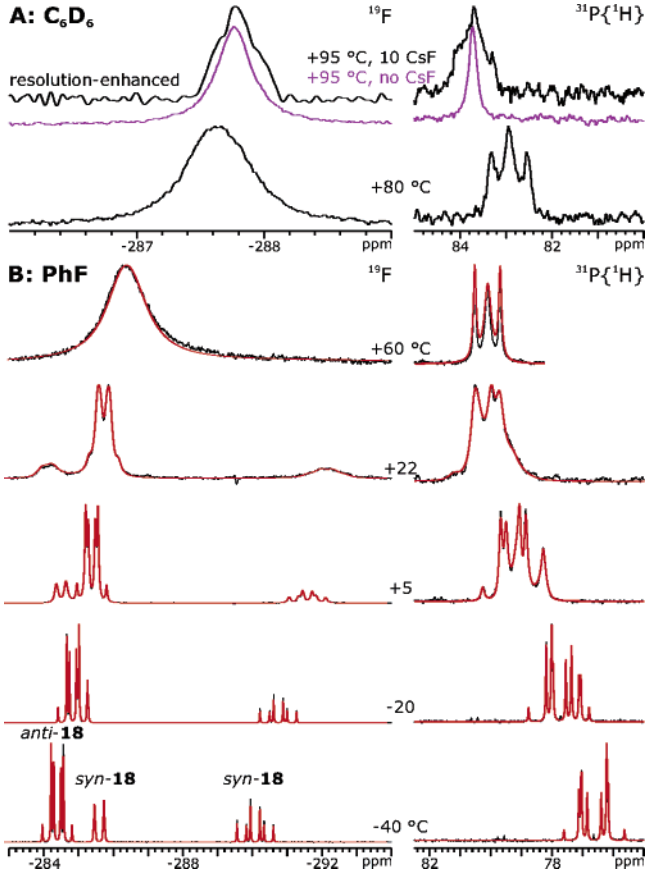

Figure 7. Variable-temperature ^{19}F and $^{31}P\{^1H\}$ spectra of **18** in PhF and C_6D_6 showing the effects of dynamic *syn*↔*anti* equilibrium. Iteratively fitted line shape is overlaid in red.

toward *syn* isomers, possessing greater dipole moments, with $K_{anti\leftrightarrow syn}$ at 22 °C equal to 0.63 (C_6D_6), 1.18 (CD_2Cl_2) for **17** and 0.14 (C_6D_6), 0.41 (PhF), 0.46 (CD_2Cl_2) for **18**. Hindered rotation of P(*o*-Tolyl)$_3$ ligands[49] in **17** complicates the observed line-broadening effects and restricts the amount of spectroscopic data available for *anti*- and *syn*-**17** isomers to those shown in Scheme 1. Observation of ordinary overlapping doublets in $^{31}P\{^1H\}$ spectrum of **17** at 22 °C limits J_{FF} coupling in *anti*-**17** to ≤60 Hz, so as to conceal second-order effects in the line width. As the temperature is raised, spectra of **17** undergo sharpening, due to accelerated rotation of P(*o*-Tolyl)$_3$, followed by broadening resulting from *anti*↔*syn*-**17** interconversion; latter is most clearly indicated by the coalescence of *o*-Me signals of respective isomers in ^1H NMR spectra. Line shape analysis of 60 °C spectra yielded an exchange rate constant of 6×10^1 s^{-1} that corresponds to $\Delta G_{60°}^{\ddagger} = 17$ kcal/mol.

Complex **18** does not suffer complications from hindered rotation of P(*t*-Bu)$_3$ in the examined temperature range, which enabled a more extensive solution characterization. Low-temperature ^{19}F and $^{31}P\{^1H\}$ NMR spectra clearly revealed the expected AA′XX′ patterns for *anti*-**18**, overlapped by ABX_2 patterns of *syn*-**18**. Both *syn*- and *anti*-**18** feature J_{FF} coupling constants (103, 120 Hz) substantially larger than those reported for PCy_3 and P^iPr_3 (60, 63 Hz) analogs[26g] of *syn*-**18**. Raising the temperature led to broadening and eventual coalescence of both $^{31}P\{^1H\}$ and ^{19}F NMR signals of *syn*- and *anti*-**18**, with

Scheme 2. Solution Dynamics Exhibited by **17** and **18**

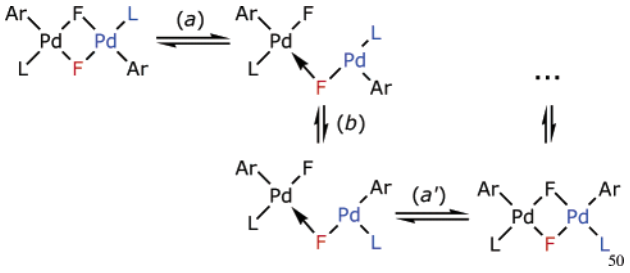

both spectra exhibiting notable broadening already at 22 °C. Retention of J_{PF} coupling, at its population-weighed exchange-averaged value, in the high-temperature limit (Figure 7) identifies this dynamic process as the *anti*↔*syn*-**18** interconversion. Rate constants in several solvents obtained from iterative line shape fitting yielded, from Eyring analysis (Supporting Information), $\Delta H_{syn\leftrightarrow anti-18}^{\ddagger} = 14$ kcal/mol and $\Delta S_{syn\leftrightarrow anti-18}^{\ddagger} = -4$ cal/(mol K), latter being expectedly small for an intramolecular process (Scheme 1). The free energy barrier to *anti*↔*syn* exchange, $\Delta G_{+60°}^{\ddagger}$, in **18** is lower than that in **17** by 1.6(3) kcal/mol. The minimal physical process manifested in line-broadening and coalescence of NMR signals of *syn*- and *anti*-isomers of **17** and **18** and whose activation parameters are determined from the Eyring plots corresponds to cleavage of a single Pd−F bond (*a*, *a*′, ...) necessarily combined with isomerization of the resulting T-shaped intermediate (*b*, Scheme 2), which serves to exchange A/A′ and X/X′ sites. Because isomerization of T-shaped d^8 ML_3 complexes is facile in the absence of strong driving force effects,[50] the obtained activation parameters ($\Delta H_{syn\leftrightarrow anti}^{\ddagger}$, $\Delta G_{syn\leftrightarrow anti}^{\ddagger}$) can be taken as close upper estimates on the values corresponding to single Pd−F bridge cleavage.[51]

Initial VT NMR experiments in which samples of **18** were maintained at elevated temperatures for extended periods of time in fact showed complete loss of J_{PF} coupling at +80 °C in PhF and +95 °C in C_6D_6 (Figure 7A). As shown in the Supporting Information, spectra of these thermolyzed samples retained some degree of line-broadening on cooling back to 22 °C. However, addition of 10 equiv of CsF to these samples restored the line shape observed originally at 22 °C and further enabled direct observation of the exchange-averaged J_{PF} in the ^{19}F and $^{31}P\{^1H\}$ spectra at the +95 °C temperature limit, recorded immediately after the minimum time required for temperature equilibration of the samples in the pre-heated NMR probe. Given that accompanying high-*T* °C ^1H NMR spectra featured a single J_{PH} coupling in one of the two signals of C_6H_4-4-NO_2 in the absence or presence of CsF, including spectra of **17** at the high-*T* °C limit of +80, {Ar−Pd-L} unit remains stoichiometrically intact on the NMR time scale ($\tau > 0.2$ s) up to +95 °C in **18** and +80 °C in **17**. The loss of J_{PF} coupling in **18** and its reestablishment on treatment with CsF can therefore be attributed to formation of trace quantities of HF from decomposi-

(49) Notheis, J. U.; Heyn, R. H.; Caulton, K. G. *Inorg. Chim. Acta.* **1995**, *229*, 187−193.

(50) (a) Thorn, D. L.; Hoffmann, R. *J. Am. Chem. Soc.* **1978**, *100*, 2079−2090. (b) Romeo, R.; Minniti, D.; Lanza, S. *Inorg. Chem.* **1979**, *18*, 2362−2368. (c) Komiya, S.; Albright, T. A.; Hoffmann, R.; Kochi, J. K. *J. Am. Chem. Soc.* **1976**, *98*, 7255−7265. (d) Kayaki, Y.; Tsukamoto, H.; Kaneko, M.; Shimizu, I.; Yamamoto, A.; Tachikawa, M.; Nakajima, T. *J. Organomet. Chem.* **2001**, *622*, 199−209.

(51) It appears reasonable to expect bridge cleavage leading to the formation of a T-shaped PdAr(μ-F)L fragment with L trans to the vacant site to proceed in a concerted manner with its isomerization to the more sterically stable geometry with Ar trans to the vacant site, i.e. that processes *a*′ and *b* in Scheme 2 and the like occur together in a single elementary step.

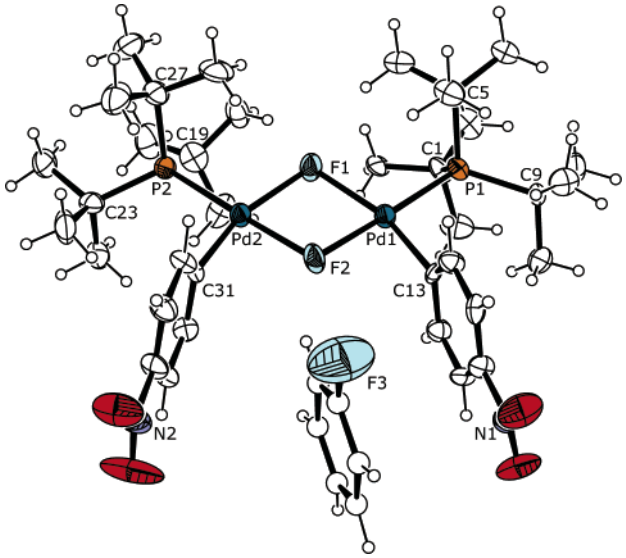

Figure 8. ORTEP drawing (50% probability ellipsoids) of the crystal structure of **18** showing the intercalated molecule of PhF. All heavy atoms were refined anisotropically. Selected geometrical parameters (Å, deg): Pd(1)−C(13), 1.944(7); Pd(2)−C(31), 1.929(7); Pd(1)−F(2), 2.080(4); Pd(2)−F(2), 2.078(4); Pd(1)−F(1), 2.140(4); Pd(2)−F(1), 2.120(4); Pd(1)−P(1), 2.283(2); Pd(2)−P(2), 2.279(2); F(2)−Pd(1)−F(1), 76.00(15); F(2)−Pd(2)−F(1), 76.48(15); C(13)−Pd(1)−P(1), 97.3(2); C(31)−Pd(2)−P(2), 98.5(2); F(1)−Pd(1)−P(1), 102.39(12); F(1)−Pd(2)−P(2), 100.50(12); Pd(2)−F(1)−Pd(1), 101.84(16); Pd(2)−F(2)−Pd(1), 105.39(17).

Scheme 3. Proposed Intermolecular F^- Exchange in **18** Mediated by HF

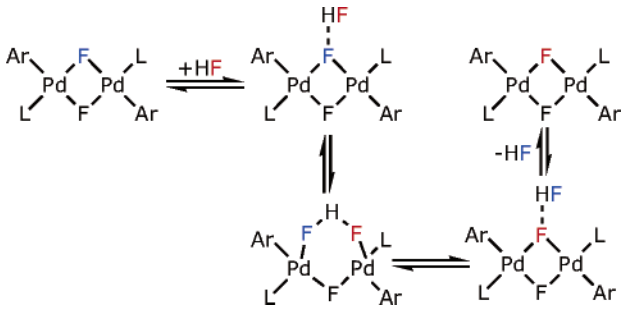

tion of **18** on thermolysis (vide infra). One mechanism by which J_{PF} coupling in **18** could be lost with help of HF is the intermolecular F^- exchange, possibly proceeding with minimal disruption of F^--bridged dimer structure as shown in Scheme 3.

These high-temperature NMR studies thus offer no conclusive evidence for complete dimer cleavage. Broadening of the limiting 63 Hz binomial triplet in the 95 °C $^{31}P\{^1H\}$ spectrum (Figure 7A), though likely due to traces of HF, limits the lifetime of the two monomers connected via at least one bridge to at least ∼1/(50 Hz) or $\tau > 20$ ms and complete dimer dissociation $\Delta G_{+95°C}^{\ddagger} > 19$ kcal/mol.

X-ray Structure of *syn*-18×(PhF)$_2$. Dimeric nature of **18** was substantiated further by a crystal structure determination (Figure 8).[52] **18** crystallizes from PhF at −35 °C as the minor, *syn*-isomer with two PhF molecules per dimer that form separate extended hydrogen-bonded networks and suffer from minor positional disorder. One of the PhF molecules participates in a peculiar π-stacking interaction with one of the C_6H_4-4-NO_2 ligands (PhF···C(13)C_5H_4-4-NO_2 = 3.52 Å), protruding in the cleft between the *syn* Ar rings to the extent compatible with the (PhF)H···F(2) hydrogen bond (H···F 2.53 Å);[53] the same PhF molecule forms another (PhF)H···F(2) hydrogen bond (H···F 2.65 Å) to the F(2) site in another dimer. An intermolecular (P(*t*-Bu))CH···F(2) = 2.92 Å interaction brings the number of H···F ≤ 3.0 Å contacts to F(2) to three, whereas F(1) forms six such interactions (1.98−2.84 Å), all intermolecular with P(*t*-Bu)$_3$ hydrogens. Extensive participation of one fluoride of *syn*-**18** in hydrogen bonding with surrounding P(*t*-Bu)$_3$ C−H bonds[26g] bears direct implications for its thermal reactivity (vide infra). Severe steric repulsion between P(*t*-Bu)$_3$ and *cis*-aryl ligands is evident in the bending of aryl rings at ipso-C13, C31 by 13 and 14°, respectively, from coplanarity with Pd−C_{ipso} bonds, as well as widening of the (*t*-Bu)-P−Pd angles to the (C9)Me_3 and (C23)Me_3 groups to 120°. Despite the notable distortions, five short CH···C(Ar) contacts remain between the P(*t*-Bu)$_3$ hydrogens and C_6H_4-4-NO_2 carbons, ranging from 2.31 to 2.54 Å. Of the total of 12 structures with P(*t*-Bu)$_3$ bound in a square-planar coordination environment available from CSD,[54] the only one with a *cis*-aryl ligand[55] shows similar bending of the Ph group from coplanarity with Pd−C_{ipso}, by 8°. Pd−F bond distances (2.078(4)···2.140(4) Å) in *syn*-**18** compare well with those in the other two structurally characterized fluoride-bridged dimeric Pd complexes (2.0984(8)···2.1336(11) Å).[26g]

2. Thermal Reactivity of [Pd(C_6H_4-4-NO_2)L(μ-F)]$_2$. L = P(*o*-Tolyl)$_3$, 17. Thermolysis of **17** in C_6D_6 at 60 °C required near a week for complete conversion and resulted in a mixture of reductively coupled and protolyzed aromatic compounds originating from both Ar═C_6H_4-4-NO_2 and *o*-Tolyl substituents of the phosphine (Scheme 4).[56] PdL_2[47a] formed and decayed as the only identifiable intermediate. In addition to large quantities of Pd^0 and free L = P(*o*-Tolyl)$_3$, the resulting mixture contained a minor amount of PF_2(*o*-Tolyl)$_3$[57a] (∼10% in F, ^{19}F NMR), whereas GC-MS and ESI-MS also indicated presence of P(*o*-Tolyl)$_2$Ar, PF_2(*o*-Tolyl)$_2$Ar and complete absence of phosphonium P(*o*-Tolyl)$_3$Ar$^+$ (after redissolution in $CDCl_3$) or the desired Ar−F. Qualitatively, the observed organic products signify two key processes dominating thermal reactivity of **17** (Scheme 4): (*p*) F/Ar ligand redistribution[58] followed by reductive elimination of Ar−Ar from the Pd(Ar)$_2$L fragment, and (*q*) Pd−Ar/P-(*o*-Tolyl) aryl group exchange[46,26e] producing (*o*-Tolyl)-analogs of {Pd}Ar intermediates and leading to

(52) Crystallographic details for [Pd(C_6H_4-4-NO_2)P(*t*-Bu)$_3$(μ-F)]$_2$ × (PhF)$_2$ (**18** × (PhF)$_2$), $C_{48}H_{72}F_4N_2O_4P_2Pd_2$, 1091.82 g/mol, Monoclinic, $P2_1/n$, a = 15.473(4), b = 12.450(3), c = 26.373(7), β = 100.704(4)°, V = 4992(2) Å^3, T = −99 °C, Z = 4; $R1$ = 0.0450, w$R2$ = 0.0901 ([$I > 2\sigma(I)$]); $R1$ = 0.0857, w$R2$ = 0.1028 (all data); GOF = 1.018.

(53) C−H bonds were extended to 1.083 Å for all reported H···X measurements.
(54) *The Cambridge Structural Database*, version. 5.27, November 2005; The Cambridge Crystallographic Data Centre: Cambridge, U.K., 2006.
(55) Liu, X.; Hartwig, J. F. *Org. Lett.* **2003**, *5*, 1915−1918.
(56) All yields are given in Pd equivalents, i.e. 1 mol of Ar−Ar formed per 1 mol of Pd dimer corresponds to 100%. Products quantified in Schemes 4 and 5 were identified directly in the reaction mixtures by NMR and quantified by integration vs internal standard (± 5%). Products identified by GC-MS only may have originated from additional thermal reactivity at T °C of up to 280 during GC analysis. See Supporting Information for additional details.
(57) (a) Holmes, R. R.; Holmes, J. M.; Day, R. O.; Swamy, K. C. K.; Chandrasekhar, V. *Phosphorus, Sulfur Silicon Relat. Elem.* **1995**, *103*, 153−169. (b) Herrmann, W. A.; Brossmer, C.; Reisinger, C.-P.; Riermeier, T. H.; Öfele, K.; Beller, M. *Chem.−Eur. J.* **1997**, *3*, 1357−1364. (c) Crozet, M. P.; Vanelle, P. *Tetrahedron Lett.* **1985**, *26*, 323−326. (d) Fild, M.; Schmutzler, R. *J. Chem. Soc., A* **1970**, 2359−2364. (e) Durà-Vilà, V.; Mingos, D. M. P.; Vilar, R.; White, A. J. P.; Williams, D. J. *J. Organomet. Chem.* **2000**, *600*, 198−205.
(58) Cárdenas, D. J.; Martín-Matute, B.; Echavarren, A. M. *J. Am. Chem. Soc.* **2006**, *128*, 5033−5040.

Scheme 4. Thermal Reactivity of **17**: Identified Products with Their Yields (Left) and Proposed Reaction Pathways (Right)

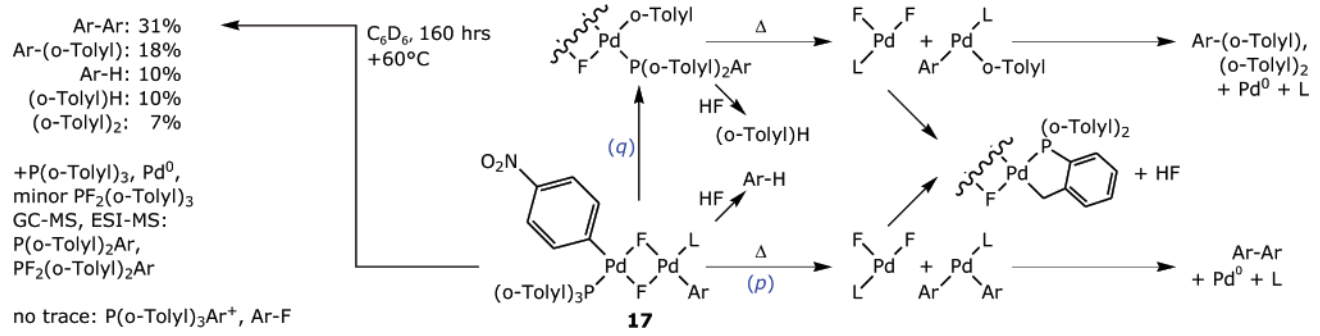

Scheme 5. Thermal Reactivity of **18**: Identified Products with Their Yields (Left) and Proposed Reaction Pathways (Right)

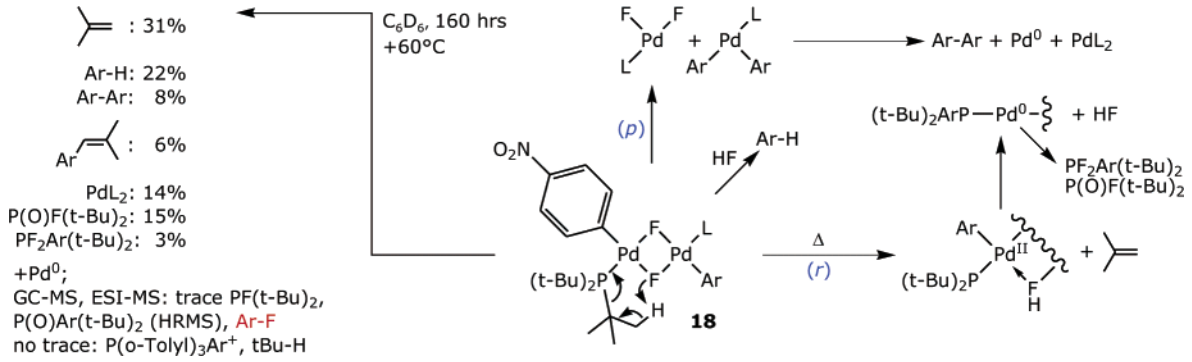

corresponding (*o*-Tolyl)-derived organic products. The Pd(II) coproduct of (*p*), {PdF_2L}, appears to react by metalation forming analogs of (poorly soluble) Herrmann's dimers,[57b] rather than F^--mediated P(III)/Pd(II)→P(V)/Pd(0) intramolecular redox[21b,26e,g,h,30] judging from the low yield of PF_2(*o*-Tolyl)$_3$ alone[59] and the lack of any other appreciable ^{19}F signals.[60] The HF released during *o*-Tolyl metalation at this, or possibly any other {Pd}F(P(*o*-Tolyl)$_3$) stage, serves as a proton source in the formation of Ar−H and (*o*-Tolyl)H. *o*-Tolyl metalation would also be consistent with the observed H↔D exchange with C_6D_6 solvent, proceeding to the extent of ∼4.5 hydrogens per Pd, at least as a means to introduce reactive H into the system. If the *o*-Tolyl groups of the observed organic products are considered equivalent to the original Ar, exchanged via (*q*), the Ar balance observed in the 60 °C reaction is 77%. At 80 °C, thermolysis of **17** requires under 60 h to completion and yields the same products with both a decreased proportion of Ar/*o*-Tolyl exchanged products and an improved Ar balance (100 ± 10%).

Presence of iodide ions did not aid in the formation of the Ar−F reductive elimination product, as was hoped on the basis of computational results for **15** in Figure 6. **17** exchanges both fluorides for I^- with added 5 equiv. of [Bu_4N]I over an hour at RT in C_6D_6 and begins to react via pathway *p* (Scheme 4) with formation of biaryl to an appreciable extent. A 3-h thermolysis at 60 °C completes conversion of Ar into Ar−Ar (73%), Ar-(*o*-Tolyl) (18%) and (*o*-Tolyl)$_2$ (7%), with HF_2^- (70%), SiF_6^{2-} (16%) and PF_2(*o*-Tolyl)$_3$ (7%) providing a solid mass balance for the total F. Although the latter distribution is indicative of Hoffman elimination of [Bu_4N]F, produced from the halide exchange between **17** and Bu_4NI, neither free 1-butene nor Bu_3N were observed in the reaction mixture, possibly participating in coordination equilibria with the reduced Pd products formed concomitantly.

L = P(*t*-Bu)$_3$, 18. Thermolysis of **18** in C_6D_6 requires similar time to completion as does **17**, but yields a more complex mixture of products (Scheme 5). At 60 °C, isobutylene is the major organic product (≥31% measured by integration of the dissolved portion), formed together with Ar−H (22%), Ar−Ar (8%) and the Heck arylation product of isobutylene, ArCH=CMe_2[57c] (6%).[56] Pd is accounted for with PdL_2 (14%) in addition to ample Pd^0, while P(*t*-Bu)$_3$ gives rise to P(O)F(*t*-Bu)$_2$ (15%) and PF_2Ar(*t*-Bu)$_2$ (3%). With identity of P(O)F(*t*-Bu)$_2$ assured by EI-MS and close agreement of NMR data with literature,[57d] that of the novel PF_2Ar(*t*-Bu)$_2$ was established on the basis of closer agreement of its observed spectroscopic data with those of PF_2Ph(*t*-Bu)$_2$[57a] than PF_2(*t*-Bu)$_3$,[57d] a ^{19}F NMR pattern featuring coupling (J_{FH} = 2.8 Hz, from ^1H NMR) to 18 rather than 27 equiv protons and a fully assigned ^1H spectrum (Supporting Information); HRMS was additionally used to verify the elemental composition of P(O)Ar(*t*-Bu)$_2$ observed in ESI-MS and GC-MS of the reaction mixture. The predominant reactivity mode of **18** thus appears to be γ-hydrogen elimination from coordinated P(*t*-Bu)$_3$ (*r*), with bridging fluoride functioning as a base (Scheme 5). Spatial proximity of numerous P(*t*-Bu)$_3$ hydrogens to F, revealed in the crystal structure of **18**, likely assists the initial proton-transfer event possibly leading to a cyclometalated {Pd}(η^{3}C,P−CH_2CMe_2P(*t*-Bu)$_2$) intermediate prior to isobutylene elimination. Such metalation followed by isobutylene elimination was thoroughly documented as part of thermal reactivity of Ni(COD)$_2$/(*t*-Bu)$_2$NHC system.[61] Palladium phosphide {Pd^{II}}P(*t*-Bu)$_2$ intermediate resulting from isobuty-

(59) Although ESI-MS of the reaction mixture, after redissolution in $CDCl_3$, did show metalated Pd(CH_2−C_6H_4-2-P(*o*-Tolyl)$_2$)$^+$ and Pd(CH_2−C_6H_4-2-P(*o*-Tolyl)$_2$)(P(*o*-Tolyl)$_3$)$^+$ fragments, their presence in ESI-MS spectrum is typical of many Pd(P(*o*-Tolyl)$_3$) complexes, i.e. metalation takes place readily during ESI.

(60) A reviewer suggested PF_2(*o*-Tolyl)$_3$ to react with low-ligated, highly reactive Pd(0) species instead.

(61) Caddick, S.; Cloke, F. G. N.; Hitchcock, P. B.; Lewis, A. K. de K. *Angew. Chem., Int. Ed.* **2004**, *43*, 5824−5827.

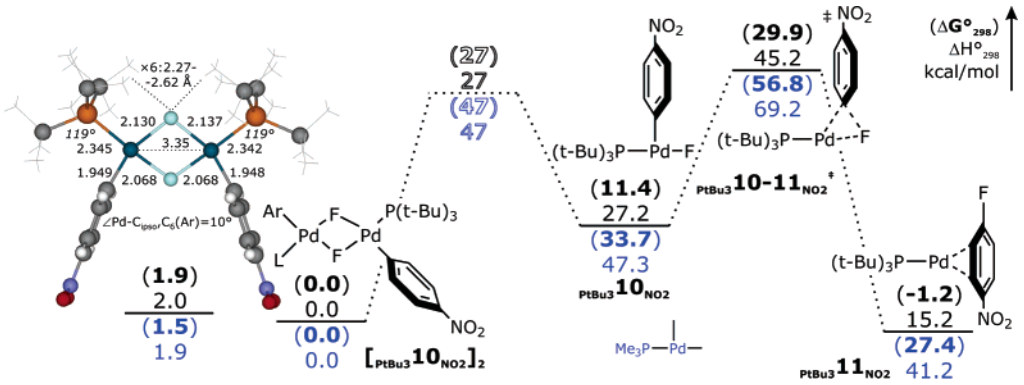

Figure 9. Computed structure of *syn*-**18** and reactivity profiles of [Pd(C$_6$H$_4$-4-NO$_2$)(L)(μ-F)]$_2$ (L = P(*t*-Bu)$_3$, **[$_{PtBu_3}$10$_{NO_2}$]$_2$**; L = PMe$_3$, **[10$_{NO_2}$]$_2$**, in blue).

lene/HF elimination in the case of **18** could ostensibly undergo 1,2-migration[30d] of Ar from Pd to furnish the modified phosphine P(C$_6$H$_4$-4-NO$_2$)(*t*-Bu)$_2$, or that of a fluoride to yield PF(*t*-Bu)$_2$, traces of which were identified by GC-MS. The novel PAr(*t*-Bu)$_2$ thus formed can be correlated to the observed PF$_2$Ar(*t*-Bu)$_2$ via F$^-$-mediated P(III)/Pd(II)→P(V)/Pd(0) intramolecular redox,[21b,26e,g,h,30] with hydrolysis of PF$_2$Ar(*t*-Bu)$_2$ or-{Pd^{II}}P(*t*-Bu)$_2$ by adventitious moisture possibly responsible for the formation of P(O)F(*t*-Bu)$_2$. Repeating the reaction at 80 °C for 60 h increased the PF$_2$Ar(*t*-Bu)$_2$: P(O)F(*t*-Bu)$_2$ ratio from 1:5 to 6:4 of the same total. Containment of the reaction mixture in a Teflon NMR tube liner produced nearly identical results, yet in the presence of 10 equiv. of CsF in an all-glass NMR tube at 80 °C formation of the oxofluorophosphorane was strongly suppressed, PF$_2$Ar(*t*-Bu)$_2$:P(O)F(*t*-Bu)$_2$ = 9:1. These results suggest adventitious water associated with solid sample of **18**, rather than that from glass etching with HF and adsorbed by added CsF, as the source of P(O)F(*t*-Bu)$_2$ oxygen. Notably, volatiles vacuum-transferred from the reaction mixture contained no trace of isobutane, which necessitates hydrolysis of PF$_2$Ar(*t*-Bu)$_2$ to be selective for the formation of H−Ar or, more likely, that P−O bond formation takes place at the {Pd^{II}}P(*t*-Bu)$_2$ phosphido stage in a reaction parallel and competing with formation of P(C$_6$H$_4$-4-NO$_2$)(*t*-Bu)$_2$. Formation of the other key products, Ar−Ar and Ar−H, can be envisioned to proceed in the same manner as in the case of **17**, with the added possibility of PAr(*t*-Bu)$_2$ supporting Pd during the F/Ar ligand redistribution (*p*). Still, the observed products summarized in Scheme 5 amount to a mass balance of Ar of only 38% in the 60 °C reaction, which increases to 48% in the 80 °C/60 h run. Other products of thermolysis of **18**, featured in complex and numerous aromatic ^{1}H NMR patterns remain to be identified. Most importantly however, a trace of the desired Ar−F (~0.05%) could be identified with certainty by EI-MS in the GC-MS of several 80 °C reaction mixtures.[56]

18 shows no appreciable reactivity with 4 equiv of [Bu$_4$N]I in C$_6$D$_6$ over several hours at RT but cleanly yields Ar−Ar (92.2%), HF$_2^-$ (76.2%), and SiF$_6^{2-}$ (26.2%) after 3 h at 60 °C. Ample free 1-butene and Bu$_3$N are seen by ^{1}H NMR of the product mixture, with PdL$_2$ and [Pd^{I}L(μ-I)]$_2$[57e] accounting for all signals in ^{31}P{^{1}H} spectrum together with a minor peak at 91.3 ppm. These observations show **18** to undergo halide exchange of Pd−F with added I$^-$, followed by I$^-$/Ar ligand redistribution (*p*) in PdAr(I)P(*t*-Bu)$_3$ and reductive elimination of Ar−Ar, and Hoffman elimination of [Bu$_4$N]F, instead of the anticipated Ar−F reductive elimination from the palladate analog of **15** (Figure 6).

Computational Analysis of [$_{PtBu_3}$10$_{NO_2}$]$_2$ Reactivity. The failure of Pd(C$_6$H$_4$-4-NO$_2$)F(P(*t*-Bu)$_3$) to produce Ar−F by reductive elimination to a significant extent, as was expected on the basis of computational results, was predetermined by the exceeding stability of the fluoride-bridged dimer **18** to complete dissociation into monomers. High-temperature NMR studies (vide supra) produced activation parameters for intramolecular rearrangement involving cleavage of one bridge at a time, but gave no conclusive evidence with regard to kinetics of complete dimer breakup at +95 °C other than that it remains slow on the NMR time scale (τ > 20 ms, $\Delta G_{+95°C}^{\ddagger}$ > 19 kcal/mol). Calculations provided this insight, with faithful ONIOM models of **18**, **[$_{PtBu_3}$10$_{NO_2}$]$_2$** (Figure 9) reproducing quite well both the key geometric parameters observed in the crystal structure of *syn*-**18**, including bending of the aryl rings and *t*-Bu groups and multiple short H···F contacts between P(*t*-Bu)$_3$ hydrogens and F(1), as well as the near ergoneutrality of the *syn* and *anti*-isomers. If the activation free energy for dissociation of **[$_{PtBu_3}$10$_{NO_2}$]$_2$** into two molecules of **$_{PtBu_3}$10$_{NO_2}$**, $\Delta G^{\ddagger}$(-**[$_{PtBu_3}$10$_{NO_2}$]$_{2\rightarrow1}$**), is approximated by the dissociation $\Delta H°$, which is equivalent to $\Delta G^{\ddagger}$ for dimerization being primarily entropic in origin, kinetics of Ar−F elimination from **[$_{PtBu_3}$10$_{NO_2}$]$_2$** via the two-step process depicted in Figure 9 can be evaluated explicitly. Steady-state rate expression for the loss of **[$_{PtBu_3}$10$_{NO_2}$]$_2$** is bound by two limiting forms, a first-order dependence with rate-limiting dimer dissociation step and a half-order rate dependence on concentration of **[$_{PtBu_3}$10$_{NO_2}$]$_2$**, in which **$_{PtBu_3}$10$_{NO_2}$** is formed in a rapid pre-equilibrium and undergoes reductive elimination as the rate-determining step.[62] The activation free energy, observed in at least the initial stages, is the higher of $\Delta G_1^{\ddagger}$ = $\Delta G^{\ddagger}$(**[$_{PtBu_3}$10$_{NO_2}$]$_{2\rightarrow1}$**) and $\Delta G_{1/2}^{\ddagger}$ = [1/2 $\Delta G°$(-**[$_{PtBu_3}$10$_{NO_2}$]$_{2\rightarrow1}$**) + $\Delta G^{\ddagger}$(**$_{PtBu_3}$10−11$_{NO_2}$**‡) + *RT*ln2], for the limiting first- and half-order rate dependence respectively. Adoption of either limit is subject to the magnitude of the term a = $16k_1k_{-1}/k_2^2$ = 4 exp(−2[$\Delta G_1^{\ddagger}$− $\Delta G_{1/2}^{\ddagger}$]/RT), with $a \ll$ 1/[**18**] and $a \gg$ 1/[**18**] producing first- and half-order kinetics, respectively. Thus, ONIOM data in Figure 9 predict reductive elimination of Ar−F from **18** to be rate-limited by the initial dimer dissociation (a × [**18**] = 0.0001 at 80 °C and 20 mM initial[**18**]), with $\Delta G_{obs}^{\ddagger}$ = $\Delta G^{\ddagger}$(**[$_{PtBu_3}$10$_{NO_2}$]$_{2\rightarrow1}$**) ≈ $\Delta H°$(-**[$_{PtBu_3}$10$_{NO_2}$]$_{2\rightarrow1}$**) = 27 kcal/mol. Partial cleavage of **18**, whose

(62) Espenson, J. H. *Chemical Kinetics and Reaction Mechanisms*, 2nd ed.; McGraw-Hill: New York, 1995; p 82.

$\Delta H^\circ \leq \Delta H_{syn \leftrightarrow anti-\mathbf{18}}{}^{\ddagger} = 14$ kcal/mol (Scheme 1), could offer a more facile pathway to the overall Ar−F reductive elimination only if the (unobserved) singly bridged dimer is unstable by $\Delta H^\circ < 9$ kcal/mol relative to **18**, because reductive elimination from either of the dimer parts connected via a single F^- bridge would require an additional $\Delta H^{\ddagger} > \Delta H^{\ddagger}(\mathbf{_{PtBu_3}10-11_{NO_2}}^{\ddagger}) = 18$ kcal/mol (Figure 5).[63] The observed reaction time scale, 60 h at 80°, implies an effective $t_{1/2} \approx 10$ h and $\Delta G_{obs}{}^{\ddagger}$ of 28.4 kcal/mol, which is close enough to the ONIOM estimate of 27 kcal/mol to suggest that the true reductive elimination barrier from **18** is not too far above that for C−H activation of P(*t*-Bu)$_3$, the predominant reactivity observed, yet high enough to afford only marginal traces of the Ar−F.[64]

Computational data for the PMe_3 analogs in Figure 9 put the effect of P(*t*-Bu)$_3$ in perspective. Intramolecular steric repulsion with P(*t*-Bu)$_3$ ligands makes dissociation of $\mathbf{[_{PtBu_3}10_{NO_2}]_2}$ 20 kcal/mol (per dimer) more favorable in ΔH° than that of $\mathbf{[10_{NO_2}]_2}$, in addition to lowering the $\Delta H^{\ddagger}$ of Ar−F reductive elimination by 3.9 kcal/mol. With the dimer dissociation predicted to be rate-limiting in the overall reductive elimination starting from the dimer $\mathbf{[10_{NO_2}]_2}$ (as well as $\mathbf{[10]_2}$ but not $\mathbf{[1]_2}$), steric bulk of P(*t*-Bu)$_3$ lowers the activation barrier of PMe_3 analog by 20 kcal/mol. However dramatic, this reduction in $\Delta G_{obs}{}^{\ddagger}$ with P(*t*-Bu)$_3$ apparently falls short of enabling quantifiable Ar−F reductive elimination in practice.

L = P(C$_6$H$_4$-2-Trip)(*t*-Bu)$_2$. Recent studies by Buchwald et al. demonstrated a range of rather unique catalytic reactivity of Pd complexes supported by this and related derivatives of P(*t*-Bu)$_3$, including the unprecedented synthesis of phenols,[24h] broad range of aryl ethers[65a,b,24g] and hetero-biaryls[65c] among other applications. Remarkably, both **17** and **18** proceeded to yield, in separate reactions in the presence of 4 equiv of P(C$_6$H$_4$-2-Trip)(*t*-Bu)$_2$ in C_6D_6 at 60 °C over 22 h, ca. 10% of F−C$_6$H$_4$-4-NO$_2$, readily identified by ^{1}H, ^{19}F NMR, and GC-MS in comparison to authentic sample. This is the first indication, to our knowledge, of net Ar−F reductive elimination operating to a quantifiable extent from a transition metal aryl fluoride. Although a detailed study of Buchwald's P(C$_6$H$_4$-2-Trip)(*t*-Bu)$_2$ reactivity with fluoride-bridged Pd dimers is beyond the scope of this work, experimental observations at hand fit closely within the mechanistic framework of the original aryl-halide reductive elimination reactions from Pd(II)[25] that follow associative substitution of P(*o*-Tolyl)$_3$ with bulkier P(*t*-Bu)$_3$ and cleavage of halide-bridged dimers into three-coordinate monomers.[25d] The limited yet measurable success of P(C$_6$H$_4$-2-Trip)(*t*-Bu)$_2$ in enabling net Ar−F reductive elimination is therefore doubtless due to its ability to destabilize sterically the fluoride-bridged Pd dimer beyond the extent possible with P(*t*-Bu)$_3$.

(63) Both Pd fragments in the partly cleaved dimer are derived from the basic T-shaped PdAr(F)L geometry by coordination of a nucleophile to Pd or electrophile to F, modifications that were computed (Figures 2, 3) to increase the barrier to reductive elimination from that of the T-shaped precursor.

(64) Underestimation of the stability of $\mathbf{_{PtBu_3}10_{NO_2}}$ relative to $\mathbf{[_{PtBu_3}10_{NO_2}]_2}$ and $\mathbf{_{PtBu_3}10-11_{NO_2}}^{\ddagger}$ in the computational model due to inadequate description of P(*t*-Bu)CH···Pd agostic interactions (vide supra) serves to raise $\Delta G_1{}^{\ddagger}$ approximated by $\Delta H^\circ(\mathbf{[_{PtBu_3}10_{NO_2}]_{2\rightarrow 1}})$, but affects $\Delta G_{1/2}{}^{\ddagger}$ much less due to cancellation of the decrease in $\Delta H^\circ(\mathbf{[_{PtBu_3}10_{NO_2}]_{2\rightarrow 1}})$ and increase in $\Delta G^{\ddagger}(\mathbf{_{PtBu_3}10-11_{NO_2}}^{\ddagger})$; the difference from experiment introduced by the systematic error of the computational model is estimated to be on the order of 5 kcal/mol.

(65) (a) Burgos, C. H.; Barder, T. E.; Huang, X.; Buchwald, S. L. *Angew. Chem., Int. Ed.* **2006**, *45*, 4321−4326. (b) Vorogushin, A. V.; Huang, X.; Buchwald, S. L. *J. Am. Chem. Soc.* **2005**, *127*, 8146−8149. (c) Billingsley, K. L.; Anderson, K. W.; Buchwald, S. L. *Angew. Chem., Int. Ed.* **2006**, *45*, 3484−3488.

Table 2. Correlations between Activation and Equilibrium Enthalpies (kcal/mol) of Ar−F Reductive Elimination Computed for Various L$_n$Pd^{II}(Ar)F Complexes

L$_n$Pd^{II}(Ar)F	L$_n$	Ar	$\Delta H^{\ddagger}$	ΔH°	α^a (R^2)
1	Me_2NHC	Ph	28.9	1.2	0.50
$_{Cl2}$**1**	Cl_2Me_2NHC	Ph	28.0	−0.3	(0.92)
15	$(I^-)PPh_3$	Ph	26.4	−1.0	
10	PMe_3	Ph	25.1	−5.6	
$_{PPh_3}$**10**	PPh_3	Ph	24.1	−7.7	
5	η^2-$(MeNHC)_2CH_2$	Ph	50.6	22.4	
1$_{...HF}$	Me_2NHC/F...HF	Ph	39.7	13.6	
1	Me_2NHC	Ph	28.9	1.2	
5$_\eta$**1**	η^1-$(MeNHC)_2CH_2$	Ph	28.4	0.5	0.94
13	$(PMe_3)_2$	Ph	38.8	5.1	(0.96)
10	PMe_3	Ph	25.1	−5.6	
10$_{NO_2}$	PMe_3	C$_6$H$_4$−4-NO$_2$	21.9	−6.1	
$_{PtBu_3}$**10**$_{NO_2}$	P(*t*-Bu)$_3$	C$_6$H$_4$−4-NO$_2$	18.0	−12.1	
1$_{OMe}$	Me_2NHC	C$_6$H$_4$−4-OMe	30.5	1.8	2.4
1	Me_2NHC	Ph	28.9	1.2	(1.00)
1$_{NO_2}$	Me_2NHC	C$_6$H$_4$−4-NO$_2$	25.5	−0.2	
10	PMe_3	Ph	25.1	−5.6	7.0
10$_{NO_2}$	PMe_3	C$_6$H$_4$-4-NO$_2$	21.9	−6.1	
1	Me_2NHC	Ph−F	28.9	1.2	−44
7	Me_2NHC	HC(O)−F	10.5	1.7	

[a] Brønsted $\alpha \approx \partial(\Delta H^{\ddagger})/\partial(\Delta H^\circ)$.

Discussion

DFT calculations show concerted reductive elimination of Ph−F from **1**, a representative of organometallic Pd(II) intermediates featured in catalytic transformations, to be nearly thermoneutral ($\Delta H^\circ = +1.2$) and face a surmountable activation barrier, $\Delta H^{\ddagger} = 28.9$ kcal/mol. Thus, Ar−F reductive elimination in principle is an elementary C−F bond-forming reaction that can be both kinetically competitive and thermodynamically feasible in a three-coordinate Pd(II) environment.

Auxiliary ligand effects on elimination kinetics elucidated computationally can be readily rationalized with help of NBO partial charges that reveal a monotonic transfer of comparable 0.30 e^- from F^- and 0.35 e^- from Ph mainly to Pd (0.56 e^-) to accompany Ph−F elimination from **1** with an intermediate degree of bond-making/breaking and charge-transfer featured in the transition state. Such pattern of charge redistribution suggests interactions between Pd and auxiliary donor ligands, as well as those between F^- and external electrophiles, to be the strongest in the Pd(II) reactant state, containing most Lewis acidic Pd and most Lewis basic F^-, and progressively weaken on going to elimination TS and Pd(0) product. Thus, increasing the auxiliary ligand donor strength, their number, or binding instead a hydrogen-bond donor to eliminating F^- in all states of the reaction profile will all serve to decrease elimination driving force and increase activation barrier to a necessarily smaller extent. These qualitative trends can be seen in the relative activation and equilibrium enthalpies computed for the complexes grouped in the top two blocks of Table 2.

Consideration of Brønsted α parameters ($\approx \partial(\Delta H^{\ddagger})/\partial(\Delta H^\circ)$) for selected subgroups of reactions reveals additional qualitative aspects of the influence of different modifications to the coordination environment on the elimination kinetics. Thus, reduction of auxiliary ligand donor strength from Me_2NHC to PPh_3 destabilizes Pd(II) reactant and stabilizes Pd(0) product state both to a comparable extent relative to the elimination TS. Reduction of the activation barrier in this series is a consequence of increasing driving force with $\alpha = 0.50$ fraction of the latter

translating into the former. A distinct pattern of influence is found for the middle block of complexes in Table 2, with dissociation of strong donor ligands ((MeNHC)CH_2-, PMe_3) from Pd, of hydrogen bonding between eliminating F^- and HF and replacement of PMe_3 with the highly sterically demanding P(*t*-Bu)$_3$ all following a common linear correlation between $\Delta H^{\ddagger}$ and $\Delta H°$ with $\alpha = 0.94$. All of these modifications of Pd coordination sphere therefore primarily destabilize Pd(II) reactant state relative to both the elimination TS and Pd(0) product and serve to lower the elimination barrier directly. Last, variation of para-substituents of the aromatic ring and replacement of Ph with a formyl group altogether (bottom block in Table 2) produce $\Delta H^{\ddagger}/\Delta H°$ correlations with large absolute values of α ($\gg 1$) signifying predominant transition state effects. Structural similarity between TS **1**−**2**‡ and a Meisenheimer intermediate supports S_NAr-type electronic interactions between F^-, Pd, and the π^* orbital of the eliminating fragment as the origin of such substituents TS effects.

All of the identified means to promote Ar−F reductive elimination kinetics from Pd(II) environment could be potentially applied in practice. The most significant net reduction of the activation barrier results from destabilization of the square-planar $Pd^{II}Ar(F)L_2$ reagent by removal of a strong auxiliary donor ligand (Figures 2, 6; $\Delta\Delta H^{\ddagger} = -22$, -14 kcal/mol, respectively). Exclusion of intermolecular hydrogen-bond donors (Figure 3, $\Delta\Delta H^{\ddagger} = -11$ kcal/mol) and increase of steric repulsion between the eliminating Ar and the sole remaining auxiliary ligand (Figure 5, $\Delta\Delta H^{\ddagger} = -4$ kcal/mol) offer additional means to lower the activation barrier. Last, fine-tuning improvement of the elimination kinetics should be possible via lowering of auxiliary ligand donor strength (Figures 1, 5; $\Delta\Delta H^{\ddagger} = -4.8$ kcal/mol) and progressively electron-withdrawing *para*-substitution of the Ar group (Figures 1, 5; $\Delta\Delta H^{\ddagger} = -5$ kcal/mol).

However, all of the above strategies for promoting the desired Ar−F reductive elimination reactivity in practice can be useful only once measures are taken to prevent aggregation of the reactive three-coordinate $Pd^{II}Ar(F)L$ into fluoride-bridged dimer. Structural preferences in the Pd(Ar)X(Q-Phos) (X = Cl, Br, I)[47b] and Pd(Ar)X(P(*t*-Bu)$_3$) (X = Br, I)[25] series together with pronounced stability of dimeric **18** found in this study show dramatically increased propensity of three-coordinate PdAr(X)L to dimerization with lighter halides X. ONIOM calculations provide the equilibrium $\Delta H°$ for complete dissociation of the accurate model of **18**, $\mathbf{[_{PtBu_3}10_{NO_2}]_2}$ at 27 kcal/mol, and show steric effect of the bulky P(*t*-Bu)$_3$ to decrease dimer stability by 20 kcal/mol from that of the PMe_3 analog $\mathbf{[10_{NO_2}]_2}$ (Figure 9), primarily via repulsion with the *cis*-aryl ligand. It is the steric bulk of the auxiliary ligands that is therefore the key element of the Pd coordination environment that may be used to destabilize fluoride-bridged dimer geometry sufficiently for monomeric PdAr(F)L to become accessible, with only a weak, agostic stabilization of Pd introduced in place of the fluoride bridge.

Success of this approach in practice with L = P(*t*-Bu)$_3$ in **18** was ultimately limited to formation of ppm levels of the aryl fluoride product, by ligand C−H activation processes taking place in part as a consequence of close spatial proximity of the P(*t*-Bu)$_3$ hydrogens to bridging fluoride(s). Surprisingly however, use of Buchwald's P(C_6H_4-2-Trip)(*t*-Bu)$_2$ appears to have provided the additional steric "push" needed to assist dissociation of the fluoride-bridged dimer and led to the formation of measurable quantities of the sought Ar−F. Conversely, L = P(*o*-Tolyl)$_3$ analog **17** produced no trace of Ar−F and is expected to face an even greater barrier to dissociation than **18**, based on both the 1.6(3) kcal/mol higher measured barrier to single bridge cleavage in the *syn*↔*anti* exchange (vide supra) and the direct observation of coupled equilibria involving monomeric PdPh(Br)P(*t*-Bu)$_3$ and dimeric [PdPhP(*o*-Tolyl)$_3$(μ-Br)]$_2$.[25e]

Alternative strategies for promoting Ar−F reductive elimination could involve the use of judiciously chosen, strong fourth ligands in coordinatively saturated square-planar environment stable to formation of fluoride-bridged dimer. Iodide emerged as a particularly promising direction from calculations (Figure 6), yet experimentally its addition to **17** or **18** resulted in halide exchange driven by irreversible Hoffman elimination of Bu_4-NF in C_6D_6 and considerably more facile Ar/I^- ligand redistribution[58] of the {PdAr(I)L} products leading to reductive elimination of biaryls. Still, it is possible that sufficiently inert π-acidic ligands could indeed produce a stable four-coordinate Pd(II) environment reactive by Ar−F reductive elimination. At the same time, use of NHC ligands does not appear to be immediately promising, e.g., for reasons of greater oxidative stability, due to the exceedingly facile computed Ar−NHC^+ elimination from Pd(II) geometry best suited for Ar−F reductive elimination. Furthermore, the feasibility of F^--mediated intramolecular oxidation of highly sterically demanding PR_3 by Pd(II) has yet to be confirmed. No evidence for formation of PF_2(*t*-Bu)$_3$ was obtained from reactivity studies of **18**, with C−H activation, possibly mediated by F, dominating the decomposition pathways.

Conclusions

Using computational (DFT) methods, aryl-fluoride reductive elimination is shown to be a feasible elementary C−F bond forming reaction that can take place from a three-coordinate $Pd^{II}Ar(F)L$ environment with activation energy and driving force generally compatible with synthetic applications. Loss of strong fourth ligands from Pd or hydrogen bond donors from F each results in substantial destabilization of Pd(II) reactant, as does the increase of steric interactions between Ar and L, and yields most pronounced net reductions of the activation barrier. Lowering the donor strength of L assists elimination kinetics additionally by increasing the driving force, while electron-withdrawing *para*-substituents on Ar exert a useful S_NAr-like transition state effect. The key remaining obstacle to effecting Ar−F reductive elimination in practice was shown to be stability of fluoride-bridged dimers to complete dissociation into monomers, in an experimental study of the novel [Pd(C_6H_4-4-NO_2)L-(μ-F)]$_2$ (L = P(*o*-Tolyl)$_3$, **17**; P(*t*-Bu)$_3$, **18**). Inter-ligand steric repulsion with L = P(*t*-Bu)$_3$ provided a 20 kcal/mol destabilization of dimer **18**, estimated with DFT relative to L = PMe_3, however was not sufficient to promote monomer formation to a significant extent and yield greater than trace amounts of Ar−F. Ligand (P(*t*-Bu)$_3$) C−H activation, possibly assisted by Pd-bound F^-, followed by isobutylene elimination was the predominant decomposition mode of **18** observed, while Ar/F^- scrambling and reductive elimination of Ar−Ar dominate thermal reactivity of **17**. However, use of the bulkier L = P(C_6H_4-2-Trip)(*t*-Bu)$_2$ provided the additional steric pressure

needed for dimer dissociation and resulted in formation of aryl-fluoride net reductive elimination product in low yields (10%) in reactions with both **17** and **18**.

Experimental Section

General Methods. All manipulations of air- and moisture-sensitive compounds were carried out by standard Schlenk and glovebox techniques under atmosphere of nitrogen using flame- and oven-dried glassware, including NMR tubes and inserts. Full details are provided in Supporting Information.

[Pd(C_6H_4-4-NO_2)P(*o*-Tolyl)$_3$(μ-F)]$_2$ (17). A mixture of [Pd(C_6H_4-4-NO_2)P(*o*-Tolyl)$_3$(μ-I)]$_2$[47] (880 mg, 0.667 mmol), 4 equiv of AgF (338.4 mg, 2.667 mmol), and 0.1 equiv of P(*o*-Tolyl)$_3$ (20.3 mg, 66.7 μmol) was sonicated in PhMe (20 mL) at 25 °C in the dark for 6 h, at which time NMR of an aliquot in $CDCl_3$ showed complete conversion of the starting iodide. The rusty-brown solid was filtered off with Celite, the filtrate was brought to dryness in vacuo, and the residue evacuated for overnight at RT. Trituration with 40 mL of Et_2O for several hrs at RT afforded light mustard microcrystalline solid, which was collected on a frit, washed with Et_2O at RT and dried in vacuo at +70 °C for 6 h. Yield 0.632 g (0.573 mmol, 86%), mixture of *anti*- and *syn*-isomers. ^{1}H NMR (C_6D_6, 22 °C): δ 7.63 (br, 4H, (C_6H_4-4-NO_2)$_2$), 7.47 (d, J_{HH} = 8.8 Hz, 4H, (C_6H_4-4-NO_2)$_2$), 6.95 (m, 24 × 0.38 H, P(C_6H_4-2-Me)$_3$, *syn*), 6.77 (m, 24 × 0.62 H, P(C_6H_4-2-Me)$_3$, *anti*), 2.40 (s, 18 × 0.62 H, P(C_6H_4-2-CH_3)$_3$, *anti*), 2.29 (s, 18 × 0.38 H, P(C_6H_4-2-CH_3)$_3$, *syn*). ^{31}P{^{1}H} NMR (C_6D_6, 22 °C): δ 32.8 (d, J_{PF} = 167 Hz, 2 × 0.6 P, *P*(*o*-Tolyl)$_3$, *anti*), 31.9 (d, J_{PF} = 167 Hz, 2 × 0.4 P, *P*(*o*-Tolyl)$_3$, *syn*). ^{19}F NMR (C_6D_6, 22 °C): δ −292.7 (td, J_{PF} = 167 Hz, J_{FF} = 77 Hz, 1 × 0.4 F, *trans*-(*o*-Tolyl)$_3$P−Pd-*F*, *syn*), −293 (obscured, 2 × 0.6 F, Pd*F*, *anti*), −314 (br, 1 × 0.4 F, *cis*-(*o*-Tolyl)$_3$P−Pd-*F*, *syn*). Anal. found (calcd., %) for $C_{54}H_{50}F_2N_2O_4P_2Pd_2$: C 58.51 (58.76), H 4.53 (4.57), N 2.48 (2.54).

[Pd(C_6H_4-4-NO_2)P(*t*-Bu)$_3$(μ-F)]$_2$ (18). A mixture of [Pd(C_6H_4-4-NO_2)P(*o*-Tolyl)$_3$(μ-F)]$_2$ (400 mg, 0.362 mmol) and 2.2 equiv of P(*t*-Bu)$_3$ (161.3 mg, 0.797 mmol) was stirred in PhMe (20 mL) for an hour at 25 °C, filtered through Celite, the filtrate was brought to dryness in vacuo, and the residue dried at +55 °C for 7 h. Trituration with 20 mL of Et_2O for several hrs at RT afforded pale-mustard microcrystalline solid, which was collected on a frit, washed with Et_2O at RT, and dried in vacuo at +65 °C for 4 h. Yield 0.174 g (0.193 mmol, 53%), mixture of *anti*- and *syn*-isomers. ^{1}H NMR (C_6D_6, 22 °C): δ 7.77 (br, 4H, (C_6H_4-4-NO_2)$_2$), 7.51 (s, 4H, (C_6H_4-4-NO_2)$_2$), 1.14 (d, J_{PH} = 12.8 Hz, 54 H, P(C(CH_3)$_3$)$_3$). ^{31}P{^{1}H} NMR (C_6D_6, 22 °C): δ 80.2 (second order m, br, J_{PF}(*trans*) = ±154 Hz, J_{PF}(*cis*) = ∓ 10.7 Hz, 2 P, *P*(*t*-Bu)$_3$). ^{19}F NMR (C_6D_6, 22 °C): δ −286.9 (second order m, J_{PF}(*trans*) = ±154 Hz, J_{PF}(*cis*) = ∓ 10.7 Hz, $|J_{FF}|$ = 119 Hz, 2 F, Pd*F*). Anal. found (calcd., %) for $C_{36}H_{62}F_2N_2O_4P_2Pd_2$: C 48.51 (48.06), H 7.31 (6.95), N 2.87 (3.11). X-ray quality crystals were grown from PhF solution at −35 °C.

Thermolysis Studies. Flame-dried J. Young tubes with or without Teflon inserts and an internal standard in the form of CF_3COOH/$(CF_3CO)_2O$ sealed in a glass capillary were used in a temperature-controlled oil bath, with periodic monitoring by NMR (^{1}H, ^{31}P{^{1}H} and ^{19}F) at ambient *T* °C. Products were analyzed and identified on the basis of NMR, GC-MS, and ESI-MS, following basic workup as necessary. See Supporting Information for characterization of new products and additional details.

Computational Details. All calculations were carried out with Gaussian 03 suite of programs,[66] using hybrid density functional method B3PW91[67] for QM models. No symmetry constraints were imposed throughout with a single exception of [PdPh(Me_2NHC)(μ-Cl)]$_2$ (C_2). All QM geometries were optimized under standard convergence criteria with BS I, which includes SDD quasirelativistic pseudopotentials on Pd (28), P (10), Cl (10), Br (28) and I (46 core electrons) with their associated basis sets (Pd: (8s7p6d)/[6s5p3d];[68a,b] P: (4s4p)/[2s2p]; Cl, Br, I: (4s5p)/[2s3p][68c]) augmented by polarization functions (Pd: f, 1.472;[68d] P: d, 0.387; Cl: d, 0.640; Br: d, 0.428; I: d, exponent 0.289 [68e]), and 6-31G(d,p)[68f] on H, C, N, O, F. This and larger basis sets employed Cartesian basis functions throughout. The kind of all stationary points obtained from full optimizations was confirmed via frequency analysis, which revealed zero and one imaginary frequency for ground and transition states, respectively, and was used to compute thermochemical parameters without scaling. To confirm the assigned nature of the activated complexes, all transition states were animated according to the normal mode corresponding to the imaginary frequency and representative structures were optimized to the minima they connected after perturbing the TS geometry. Detailed in Supporting Information, partial IRC calculations were used to additionally characterize the TS for reductive elimination of Ph−F from PdPh(F)(Me_2-NHC), while a series of constrained optimizations was used to explore in greater detail reductive elimination of [Me_3P−Ph]$^+$ from PdPh(F)-(PMe_3). For all BS I-optimized geometries, single-point energy calculations were performed with BS II, in which SDD pseudopotentials are used for Pd (28), Br (28) and I (46 core electrons) with the associated SDD basis set augmented by (2f1g) functions[68g] for Pd and Martin's SDB-cc-pVTZ basis sets used for Br and I,[68g] with the other atoms described by 6-311G+(2d,p) basis sets.[68h−j] Electronic energies from the BS II calculations were combined with thermochemical corrections, computed via BS I frequency analyses at STP without scaling, to produce the improved estimates of gas phase $\Delta H°$ and $\Delta G°$ presented in the Figures and text exclusively, unless noted otherwise. Solvation energies were computed for selected geometries with BS I in C_6H_6 solvent described with a conductor-like screening model CPCM[69] and UAKS atomic radii (electrostatic contributions only). Benchmark study of (*o*-Tolyl)-Br reductive elimination from Pd((*o*-Tolyl))Br(P(*t*-Bu)$_3$) additionally included single-point calculations on BS I-optimized geometries with BS III: BS II with Cl and lighter atoms described by AUG-cc-pVTZ basis sets,[68k−m] using loose SCF convergence criteria. NBO analysis[70] was done with BS I. Basis set superposition errors (BSSE) for halide-bridged dimers were computed with counterpoise procedure[71] and BS I individually, recomputed for selected dimers with BS II and extrapolated from BS I to BS II for the other, closely related structures from the computed BS II/BS I ratios chosen as benchmarks; final BS II values of BSSE for all dimers analyzed were between 1.4 and 1.7 kcal/mol.

ONIOM calculations[72] were performed with a two-layer scheme, in which PMe_3-based QM/MM model system was defined within P(*t*-Bu)$_3$-based MM real system; the difference between real and model systems in all complexes studied was confined to the phosphine ligands.

(66) Pople, J. A. et al. *Gaussian 03*, revision C.02; Gaussian, Inc.: Wallingford, CT, 2004.
(67) (a) Becke, A. D. J. *Chem. Phys.* **1993**, *98*, 5648. (b) Perdew, J. P.; Wang, Y. *Phys. Rev. B* **1992**, *82*, 284.
(68) (a) Andrae, D.; Häussermann, U.; Dolg, M.; Stoll, H.; Preuss, H. *Theor. Chim. Acta* **1990**, *77*, 123−141. (b) Andrae, D.; Häussermann, U.; Dolg, M.; Stoll, H.; Preuss, H. *Theor. Chim. Acta* **1991**, *78*, 247−266. (c) Bergner, A.; Dolg, M.; Küchle, W.; Stoll, H.; Preuss, H. *Mol. Phys.* **1993**, *30*, 1431. (d) Ehlers, A. W.; Böhme, M.; Dapprich, S.; Gobbi, A.; Höllwarth, A.; Jonas, V.; Köhler, K. F.; Stegmann, R.; Veldkamp, A.; Frenking, G. *Chem. Phys. Lett.* **1993**, *208*, 111−114. (e) Höllwarth, A.; Böhme, M.; Dapprich, S.; Ehlers, A. W.; Gobbi, A.; Jonas, V.; Köhler, K. F.; Stegmann, R.; Veldkamp, A.; Frenking, G. *Chem. Phys. Lett.* **1993**, *208*, 237−240. (f) Hariharan, P. C.; Pople, J. A. *Theor. Chim. Acta* **1973**, *28*, 213. (g) Martin, J. M. L.; Sundermann, A. *J. Chem. Phys.* **2001**, *114*, 3408−3420. (h) Krishnan, R.; Binkley, J. S.; Seeger, R.; Pople, J. A. *J. Chem. Phys.* **1980**, *72*, 650. (i) McLean, A. D.; Chandler, G. S. *J. Chem. Phys.* **1980**, *72*, 5639. (j) Frisch, M. J.; Pople, J. A.; Binkley, J. S. *J. Chem. Phys.* **1984**, *80*, 3265. (k) Woon, D. E.; Dunning, T. H., Jr. *J. Chem. Phys.* **1993**, *98*, 1358. (l) Kendall, R. A.; Dunning, T. H., Jr.; Harrison, R. J. *J. Chem. Phys.* **1992**, *96*, 6796. (m) Dunning, T. H., Jr. *J. Chem. Phys.* **1989**, *90*, 1007.
(69) (a) Barone, V.; Cossi, M. *J. Phys. Chem. A* **1998**, *102*, 1995. (b) Cossi, M.; Rega, N.; Scalmani, G.; Barone, V. *J. Comput. Chem.* **2003**, *24*, 669.
(70) (a) Glendening, E. D.; Reed, A. E.; Carpenter, J. E.; Weinhold, F. *NBO*, Version 3.1. (b) Reed, A. E.; Curtiss, L. A.; Weinhold, F. *Chem. Rev.* **1988**, *88*, 899−926.
(71) (a) Simon, S.; Duran, M.; Dannenberg, J. J. *J. Chem. Phys.* **1996**, *105*, 11024. (b) Boys, S. F.; Bernardi, F. *Mol. Phys.* **1970**, *19*, 553.

QM part was described at the B3PW91/BS I level and MM contributions were computed with UFF. Factors defining distances to link atoms in model system at high and low levels were determined from UFF (model and real) and B3PW91/BS I (model system) geometry optimizations in a representative case. Loose convergence criteria were used in problematic transition states optimizations (a rationale is provided in Supporting Information); for comparison with values obtained with pure QM models, we estimate the energy difference that resulted from using loose criteria to be under 0.1 kcal/mol. As for pure QM models, both ground and transition states optimized with ONIOM were subjected to frequency analysis that revealed the requisite zero and one imaginary frequency for the respective kinds of stationary points. Improved estimates of gas phase $\Delta H°$ and $\Delta G°$ were obtained likewise, from ONIOM/BS II//ONIOM/BS I single point calculations, while CPCM solvation energies were evaluated with B3PW91/BS I on the real system (ONIOM/BS I) geometry. BSSE's were computed with extracted QM parts.

(72) (a) Maseras, F.; Morokuma, K. *J. Comput. Chem.* **1995**, *16*, 1170−1179. (b) Svensson, M.; Humbel, S.; Froese, R. D. J.; Matsubara, T.; Sieber, S.; Morokuma, K. *J. Phys. Chem.* **1996**, *100*, 19357−19363. (c) Vreven, T.; Byun, K. S.; Komáromi, I.; Dapprich, S.; Montgomery, J. A., Jr.; Morokuma, K.; Frisch, M. J. *J. Chem. Theory Comput.* **2006**, *2*, 815−826.

Acknowledgment. This work was partially supported by the National Center for Supercomputing Applications under a developmental allocation and utilized IBM P690. We thank Dr. Dmitry V. Khoroshun for advice on ONIOM optimizations, Drs. Frederick J. Hollander and Allen G. Oliver of the UC Berkeley College of Chemistry X-ray Diffraction Facility (CHEXRAY) for collection of X-ray diffraction data, and Stanford University for funding.

Supporting Information Available: Complete reference 66, computational data; variable-temperature NMR data and details of line shape analysis; crystal data and structure refinement, atomic coordinates and equivalent isotropic displacement parameters, bond lengths and angles, and anisotropic displacement parameters for $[Pd(C_6H_4\text{-}4\text{-}NO_2)P(t\text{-}Bu)_3(\mu\text{-}F)]_2\times(PhF)_2$; and experimental details of characterization of thermolysis products of **17** and **18**. This material is available free of charge via the Internet at http://pubs.acs.org.

JA066930L